

**Proceedings of
Tenth Stapp Car Crash Conference**

November 8-9, 1966

Sponsored by:

**University of Minnesota, General Extension Division
University of California Extension, Los Angeles
Biomechanics Research Center of Wayne State University**

Hosted by:

**Air Force Missile Development Center and the
6571st Aeromedical Research Laboratory**

Conducted by:

Society of Automotive Engineers, Inc.

Impact Dynamics of Unrestrained, Lap Belted, and Lap and Diagonal Chest Belted Vehicle Occupants*

L. M. Patrick and H. J. Mertz, Jr.
Wayne State University

C. K. Kroell
Research Laboratories, General Motors Corp.

THE IMPORTANCE OF RESTRAINT SYSTEMS in reducing injuries in automobile accidents has long been recognized, and many investigations have been conducted on various systems. The Automotive Crash Injury Research division of the Cornell Aeronautical Laboratory has developed a multi-degree-of-freedom mathematical model and a computer program to permit various parameters of restraint systems to be studied analytically. One of the functions of the research reported herein is to provide experimental data to check the adequacy of the mathematical model and computer program. Dynamic load-deflection characteristics of the restraint systems, the dummy, and the impact targets together with the geometry of the dummy and the joint friction (torque) were carefully controlled to ensure identical conditions for the experi-

mental and analytical programs for the given sled acceleration pulse.

Other important objectives of the program include:

1. Comparison of the dynamics of unrestrained, lap belted, and cross chest and lap belted occupants under identical impact conditions.
2. Determination of the distribution of forces on the dummy and/or restraint system under the three restraint conditions.
3. Measurement of biaxial accelerations of the head, chest, and medial end of the femur for the three restraint conditions.

*This research was sponsored jointly by G. M. Research Laboratories and Cornell Aeronautical Laboratory.

ABSTRACT

A comparison is presented of the forces, accelerations, and kinematics of an anthropomorphic dummy for identical sled impacts for unrestrained, lap belted, and lap and diagonal chest restrained conditions. Biaxial accelerometers were mounted in the head, chest, and on the proximal end of the femur to obtain the accelerations during the impacts. Seat belt load cells were put in series with the belts at each anchor point. Biaxial load cells were positioned to be impacted by the head, chest, and each knee for the unrestrained condition and by the head and chest for the lap belted configuration. For the lap and diagonal chest restrained condition these load

cells were not used. Impacts of 10 and 20 miles per hour were made with sled stopping distance of 4 and 9 inches, respectively.

At 20 miles per hour the head struck with a force of 1580 pounds in the unrestrained mode, 600 pounds with the lap belt, and did not hit with the lap and shoulder harness. The corresponding A-P head accelerations were 80, 67, and 45 G's. The total lap belt load was 3500 pounds for the lap belt only. With the lap and cross chest combination the lap belt load was 2260 pounds and the cross chest belt load was 2245 pounds for a total load of 4505 pounds. Displacements of the hip, shoulder, and head were measured from the high speed movies and are presented graphically.

4. Measurement of the dynamic load-deflection characteristics of the restraint belts.

5. Measurement of the dynamic load-deflection characteristics of the 4-inch thick cardboard honeycomb padding used on the knee, chest, and head targets.

6. Determination of the distribution of the forces in the two restraint systems.

7. Establishment of the reproducibility of forces and accelerations under identical impact conditions.

8. Comparison of the results of impacts at 10 miles per hour with a 4-inch stopping distance and at 20 miles per hour with a 9-inch stopping distance for the three restraint conditions.

The experimental program was conducted on the G. M. Research Laboratories impact sled in the Automotive Safety Research Laboratory, College of Engineering, Wayne State University. A modified automobile seat was mounted on the sled and an Alderson dummy used as the occupant. Separate triaxial targets were used to measure the knee, chest, and head forces when applicable. Separate cross chest and lap belts were used with load cells (four) at each end of each belt. Complete data are presented to permit additional analysis to be made if other investigators so desire.

EXPERIMENTAL SETUP

The experiments were conducted on the General Motors Research Laboratories impact sled in the Automotive Safety Research Laboratory, College of Engineering, Wayne State University. Figure 1 is an over-all view of the sled, and Fig. 2 shows a close-up of the seat, dummy, and targets. Detailed information on the sled and triaxial load cells has been published by Kroell and Patrick (1)^{*}.

^{*}Numbers in parentheses designate References at end of paper.

An Alderson Model F50-AU 50th percentile anthropomorphic dummy was used as the subject in all of the experimental runs. Figure 3 is a photograph of the dummy with the chest accelerometers in place. Unbonded strain gage accelerometers were used in the head and chest. Crystal accelerometers were used on the medial end of the femur. A detailed description of the accelerometers and instrumentation is given in Table I.

The decelerating cylinder, which is an Ellis Fluid Dynamics Corporation Model E148, Serial No. 2389, produces an approximately rectangular acceleration pulse. The impact was modified by the addition of a block of wood 1 5/8 inches thick between the sled and the impact cylinder to reduce the ringing induced in the sled at impact. Further damping was accomplished by placing a piece of leather 1/4 inch thick between the wood block and the impact cylinder.

All transducer signals were taken from



Fig. 2 - Dummy, seat, and targets

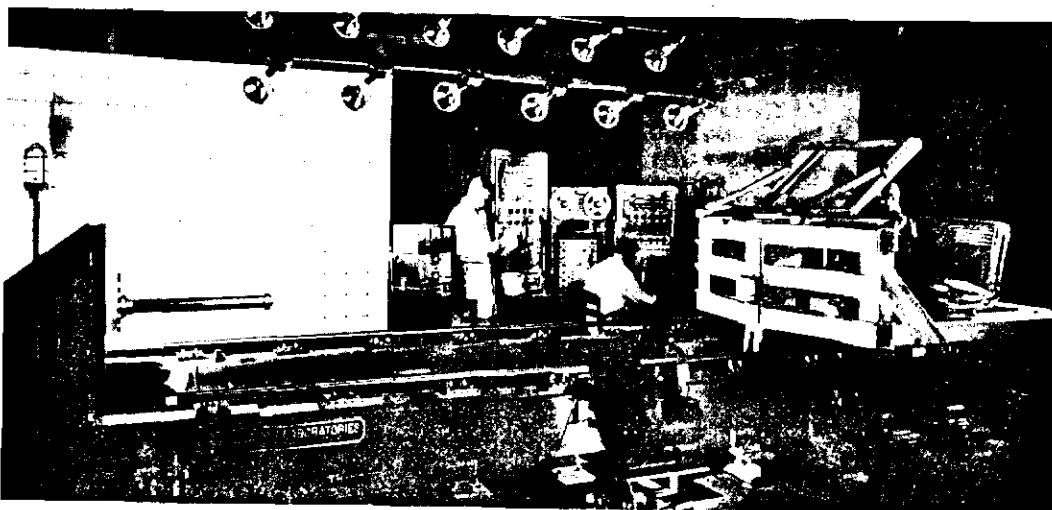


Fig. 1 - Over-all view of sled

Table 1 - Transducer, Electronic Conditioning, and Recording Details

Record	Transducer	Electronics	Galvanometer Frequency*
Head acceleration A-P direction	Statham accelerometer Model A5a-500-2700, S/N 6568	Heiland carrier amplifier Model 119-B1	3300
Head acceleration S-I direction	Statham accelerometer Model A5-100-350, S/N 10743	Heiland carrier amplifier Model 119-B1	3300
Chest acceleration A-P direction	Statham accelerometer Model A59TC-500-350, S/N 165	Heiland carrier amplifier Model 119-B1	3300
Chest acceleration S-I direction	Statham accelerometer Model A5-100-350, S/N 7741	Heiland carrier amplifier Model 119-B1	1650
Femoral axis	Endevco accelerometer Model 2215, S/N FC29	Modified Kistler charge amplifier Model 566, scale .05 mv/pcb and Kin Tel Model 111 BF	1650 1000 ohm series
Perpendicular femoral axis acceleration	Endevco accelerometer Model 2215, S/N FC58	Dyna-Monitor Model 2704	1650
Sled acceleration	Statham accelerometer Model A5-100-350, S/N 7664	Kin Tel amplifier Model 111 3F	3300
Head load cell 3-3 direction	2 axes of a triaxial strain gage load cell (G.M. and W.S.U. design)	Heiland carrier amplifier Model 119-B1	3300
Head load cell 1-1 direction		Kin Tel amplifier Model 112A	3300
Chest load cell 3-3 direction	2 axes of a triaxial strain gage load cell (G.M. and W.S.U. design)	Kin Tel amplifier Model 112A	1650
Chest load cell 1-1 direction		Heiland carrier amplifier Model 119-B1	3300
Left knee load cell 3-3 direction	1 axis of a triaxial strain gage load cell (G.M. and W.S.U. design)	Kin Tel amplifier Model 112A	1650
Right knee load cell 3-3 direction	1 axis of a triaxial strain gage load cell (G.M. and W.S.U. design)	Kin Tel amplifier Model 112A	1650
Left lap belt load cell	Strain gage load cells, compensated to measure only axial loads (W.S.U. design)	Kin Tel amplifier Model 112A	1650
Right lap belt load cell		Kin Tel amplifier Model 112A	1650
Upper shoulder harness load cell		Heiland carrier amplifier Model 119-B1	3300
Lower shoulder harness load cell		Kin Tel amplifier Model 112A	1650
Sled velocity	Magnetic pickup	None	5000

*Data were recorded on a Visicorder Model 1508 and a Visicorder Model 906A recorder.

the sled to the instrumentation consoles through a trailing cable. The cable terminated in a terminal strip from which the signals were fed to the appropriate electronic conditioning and recording equipment.

INSTRUMENTATION

The instrumentation can be divided into three categories: the instrumentation on the sled, the instrumentation on the dummy, and the photoinstrumentation.

The sled instrumentation is listed below with details provided in Table 1:

1. Velocity transducer - During the free wheeling portion of the run, two steel probes spaced 1 foot apart pass in close proximity to a magnetic pickup mounted on the frame of the sled providing timing blips on the oscillograph record.
2. A Statham Model A5-100-350 accelerometer mounted with its sensitive axis in the direction of motion of the sled.
3. A triaxial head load cell - only the two axes in the plane of motion were used.
4. A triaxial chest load cell - only the two axes in the plane of motion were used.
5. A triaxial knee load cell for each knee - only the two axes in the plane of motion were used.
6. Lap belt load cells - two for the lap belt only and four for the lap and cross chest belt runs.

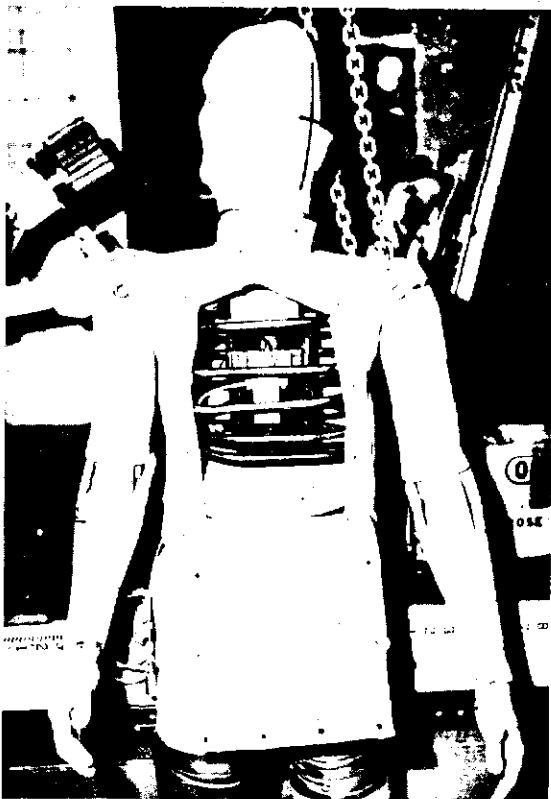


Fig. 3 - Installation of accelerometers in the chest of the dummy

The dummy instrumentation is listed below with details provided in Table 1:

1. Head acceleration A-P (anterior-posterior - front to back).
2. Head acceleration S-I (superior-inferior - top to bottom - perpendicular to A-P).
3. Chest acceleration A-P.
4. Chest acceleration S-I.
5. Femoral axis acceleration.
6. Perpendicular to femoral axis acceleration.

Photographic coverage was obtained with a Milliken Model DBM4B, Serial No. 4713, camera operated at 500 frames per second; a Photosonics Model 1B, Serial No. 12, camera operated at 1000 frames per second; and a Bell & Howell Model 70DR, Serial No. G96771, camera operated at 64 frames per second. Initial and final positions of the dummy plus other pertinent visual data were recorded with still photography. The photoinstrumentation setup is shown in Fig. 4.

A switch mounted near the track was actuated by the sled just prior to impact with the decelerating cylinder to provide a temporal relationship between the two recorders and three cameras. A 60 cycle per second timing signal was put on the records and on the camera film. Flashbulbs initiated by the same switch provide a visual record of when the switch is tripped. This provides a method for determining an exact time point on the records and on the film, while the 60 cycle signal provides a time base from the common time event of the switch.

LOAD-DEFLECTION CHARACTERISTICS OF THE BELTS

Two separate belts, one for the lap (Belt No. 4) and one for the cross chest restraint (Belt No. 2), were used to restrain the dummy during the evaluation program. Both of these belts (plus other similar belts) were evaluated dynamically to determine their load-deflection characteristics.

Dynamic loading of the belt was accomplished on the small horizontal crash simulator, Fig. 5. The sled is pneumatically accelerated to the predetermined velocity and

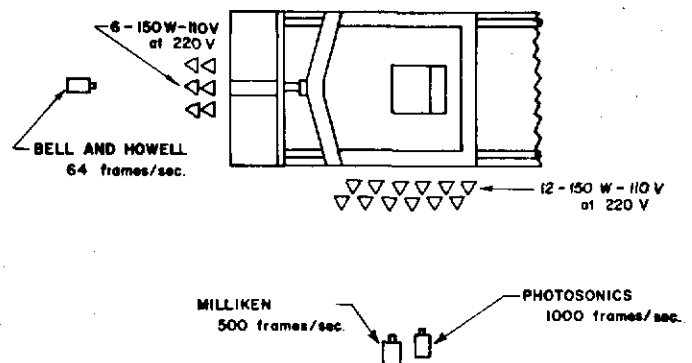


Fig. 4 - Photoinstrumentation setup

decelerated with a hydraulic device which allows control of the stopping distance and acceleration pulse shape. The fixture for loading the belt is shown mounted on the sled in Fig. 5. It consists of a block weighing 186 pounds mounted on the sled with wheels and tracks to guide it. During acceleration, the block is against a stop on the sled so it accelerates with the sled. The belt is looped around the block and its ends are attached to load cells which are affixed to the sled. Rollers are used to reduce friction

between the belt and the block. As the sled is decelerated, the block tends to continue to move forward and inertially loads the belt. A linear potentiometer provides a time-displacement record, and the load cells provide a force-displacement record. Cross plotting the records gives a force-displacement curve for the belt. A comparison of the load-deflection properties of Belts No. 2 and 4 used in these experiments is shown in Fig. 6. While the loading conditions for these belts were essentially identical (sled velocity of

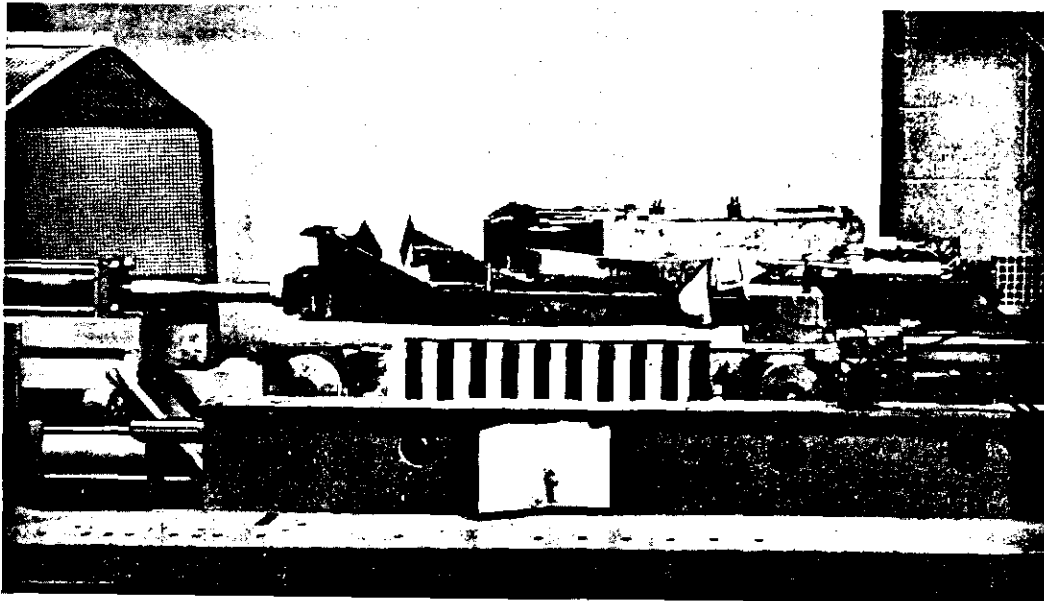


Fig. 5 - Small horizontal crash simulator with fixture for determining dynamic load-deflection characteristics of safety belts

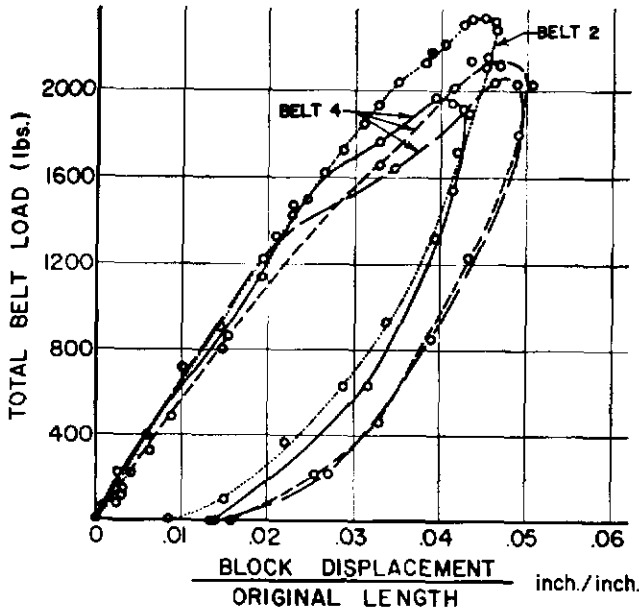


Fig. 6 - Load-deflection characteristics of Belts No. 2 and 4 used in these experiments for impacts of 23 fps and a sled stopping distance of 12 in.

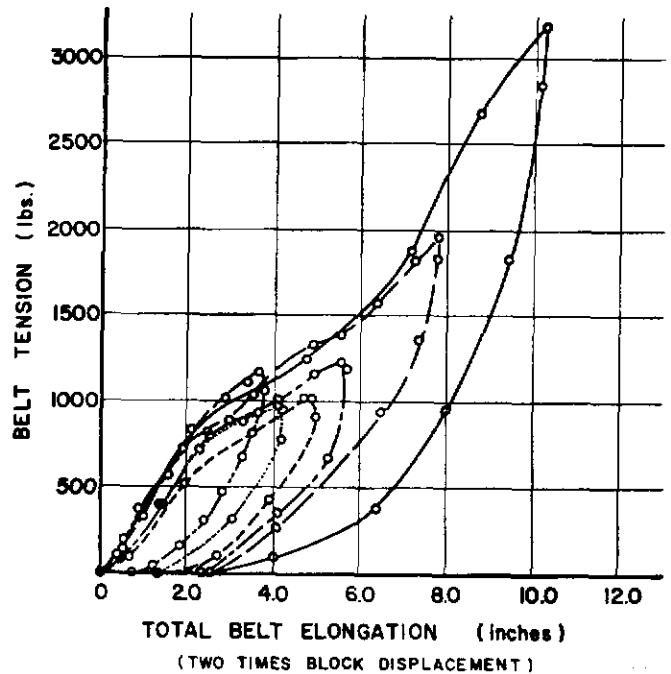


Fig. 7 - Load-unit deflection characteristics of webbing used in restraint systems

23 feet per second; stopping distance of 12 inches), the lengths of the belts were different (50 inches as compared to 42 inches).

However, by plotting the data in terms of the dimensionless parameter (unit length deflection), the total belt elongation divided by the original belt length, the load-deflection characteristics of the webbing material can be depicted by a single curve from which load-deflection characteristics for any length of belt can be determined. The load-unit length deflection characteristics of the webbing material for various loading conditions are presented in Fig. 7.

LOAD-DEFLECTION CHARACTERISTICS OF HONEYCOMB PADDING

In order to achieve a comparatively large deflection of the target, a 4-inch honeycomb material (future instrument panels and steering wheels are expected to have deflections of this magnitude) was cemented to the target and replaced after each run. The load-deflection characteristics of this material were measured statically and dynamically.

The static measurement of the load-deflection characteristics was made on a Universal test machine. The material was placed on the bed of the machine and the knee, chest, and head of the dummy, respectively, were forced into the honeycomb material. The static load-deflection characteristics for the head is shown in Fig. 8, for the chest is shown in Fig. 9, and for the knee is shown in Fig. 10. In all of these characteristic curves the initial slope is caused by the curved surface penetrating the honeycomb material with an increasing area. After maximum area is reached, the load remains approximately constant until the material bottoms out, at which time the load increases rapidly.

The dynamic load-deflection characteristics were obtained by mounting a fixture on

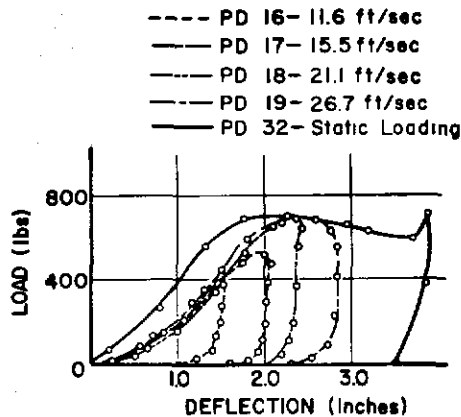


Fig. 8 - Dummy head static and dynamic load-deflection characteristics of 4 in. honeycomb material used on target including deflection of material covering head

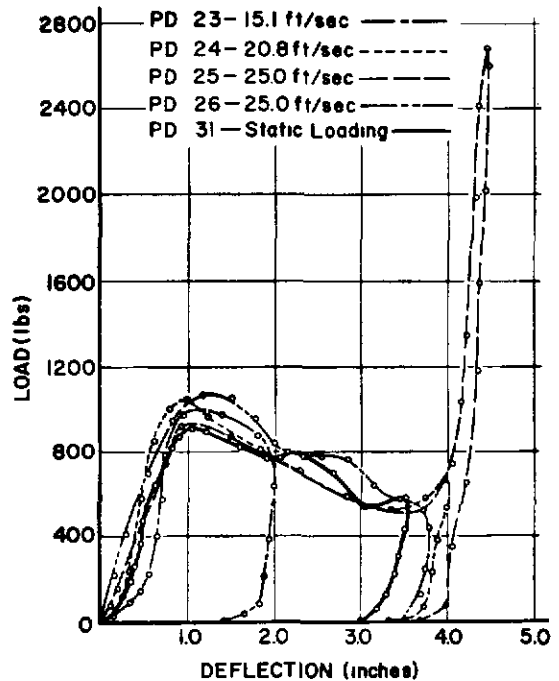


Fig. 9 - Dummy chest static and dynamic load-deflection characteristics of 4 in. honeycomb material including deflection of chest and covering material

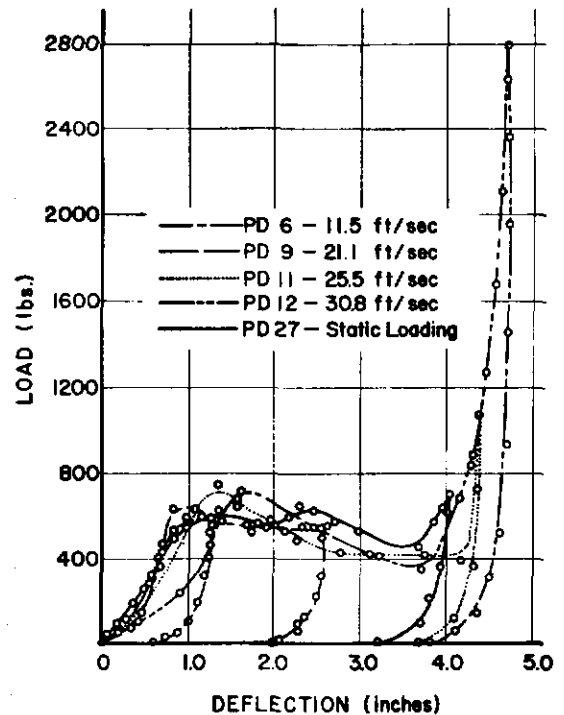


Fig. 10 - Dummy knee static and dynamic load-deflection characteristics of 4 in. honeycomb material including deflection of material covering knee

the sled as shown in Fig. 11. The target material is placed on the moving anvil while the body component is mounted rigidly to the sled in the path of the anvil and honeycomb. The sled is propelled to the desired speed and stopped by the decelerating cylinder. The anvil, which is mounted on linear ball bearings on the sled, continues forward and strikes the knee, chest, or head of the dummy. The deflection is measured by a linear potentiometer and the force is measured by the load cell on which the anvil is mounted. The dynamic load-deflection characteristics for the knee, chest, and head are shown in Figs. 8, 9, and 10 along with the static characteristics.

LOAD-DEFLECTION CHARACTERISTICS OF THE MODIFIED AUTOMOBILE SEAT

A current-production bucket seat was modified by separating the seat and seat back and by cutting away the lower corners of the seat back to provide room for the seat belt to pass between the seat and the seat back with a minimum of interference with the seat assembly. The seat cushion was stiffened in the vertical direction by installing additional spring elements to provide sufficient cushion stiffness to minimize the possibility of the seat bottoming out during the sled runs. The seat adjuster assemblies were welded in place to preclude fore and aft movement.

The vertical force-deformation characteristics of the modified seat cushion were obtained by mounting the seat on a simulated floor pan including a wooden toe board inclined at 45° in a position representing a vehicle installation. The lower portion of the dummy including the pelvis, thighs, legs, and feet was used to establish the vertical force-

deflection characteristics of the seat by applying the load through the lower portion of the dummy as shown in Fig. 12. The load was applied with a Universal test machine, and the deflection was measured on a vertical scale. Load-deflection measurements were made by applying the force through the pelvis with the H-point of the dummy at 5, 8, 11, and 14 inches, respectively, from the front beading of the seat. During all tests the center distance between the knees was held at 10 inches.

Measurement of the load-deflection characteristics in this manner included the contribution of the spring seat assembly, the cushion upholstery, and the rubber thigh and buttock material of the dummy. The zero deflection point was taken with the 42 pound dummy weight on the seat. Consequently, the total load on the seat is 42 pounds greater than the data shown in the load-deflection curves.

Some difference was noted in the load-deflection curves for the first several cycles in a given position of the dummy. This was assumed to be caused by a slight shift or repositioning of the dummy parts with each cycle. The data presented in Fig. 13 were obtained after three load cycles were made between 0 and 350 pounds to minimize the differences observed in the initial loadings. Movement of the heels during the loading cycle caused a variation in the load-deflection curves. The curves were obtained by minimizing the heel friction by manually relieving the load on the heels.

The load-deflection characteristics of the seat back were obtained by loading the seat back in the Universal test machine with the dummy torso in a manner similar to that

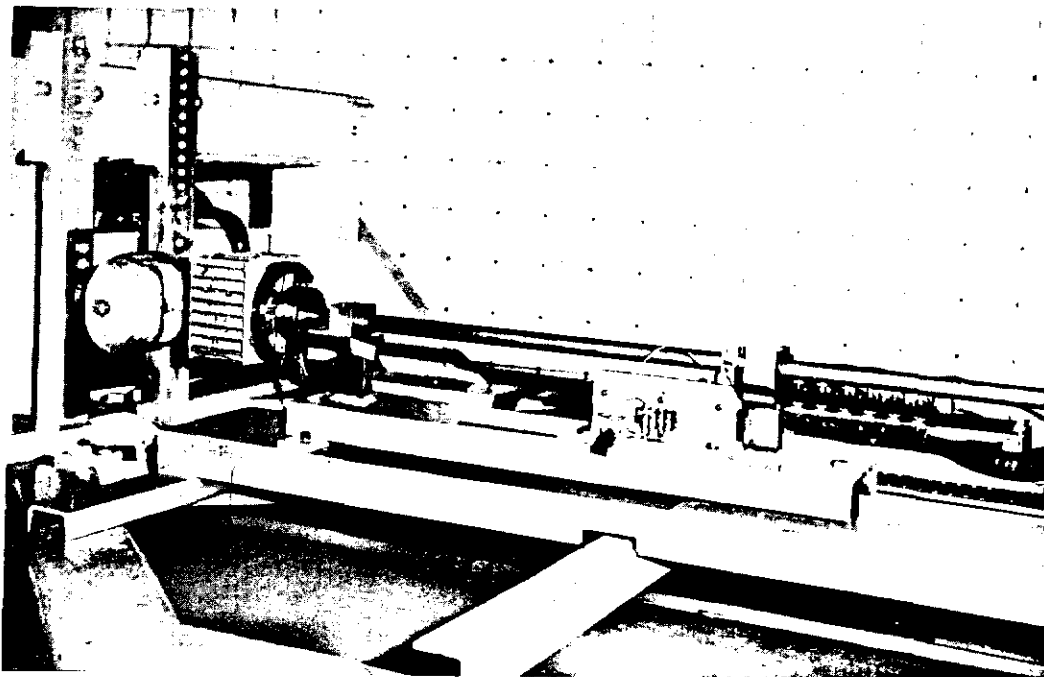


Fig. 11 - Sled fixture for measuring load-deflection characteristics of 4 in. honeycomb material

used in the seat tests. Considerable variation was observed between the load-deflection results depending on the orientation or movement of the dummy's body during or between loading cycles. The load-deflection curve for the seat back with the torso in the posi-

tion assumed to be close to that in the sled runs is shown in Fig. 14.

PROCEDURE

The dummy was located in the seat with care taken to ensure each of the dimensions

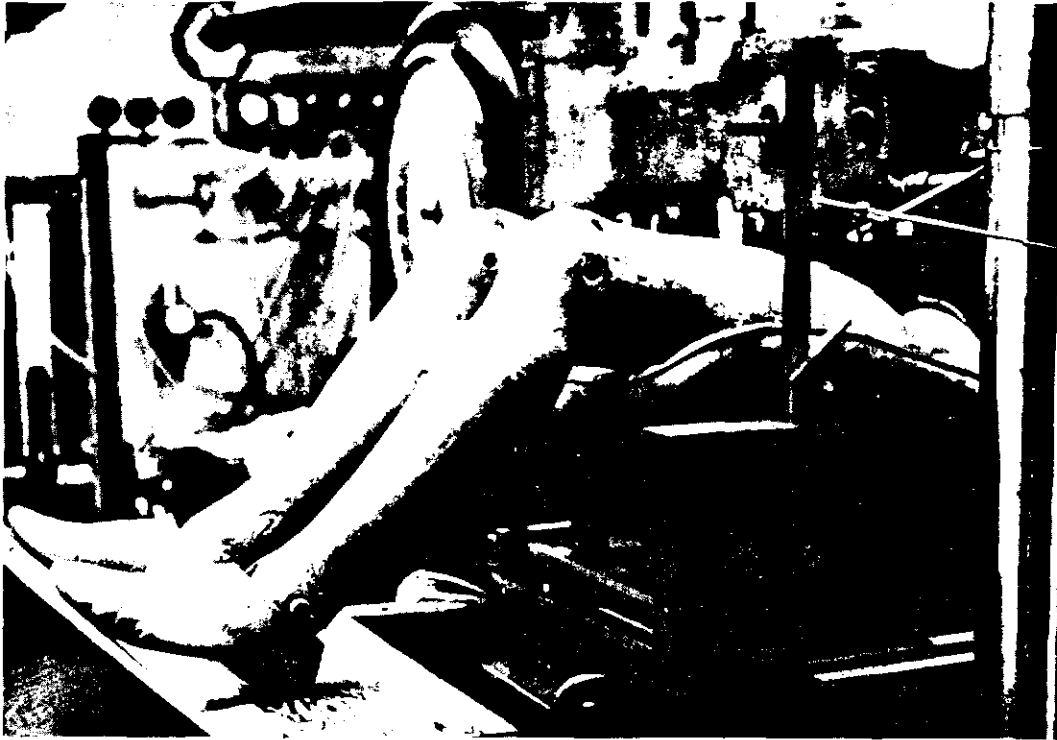


Fig. 12 - Setup for determining load-deflection characteristics of the seat

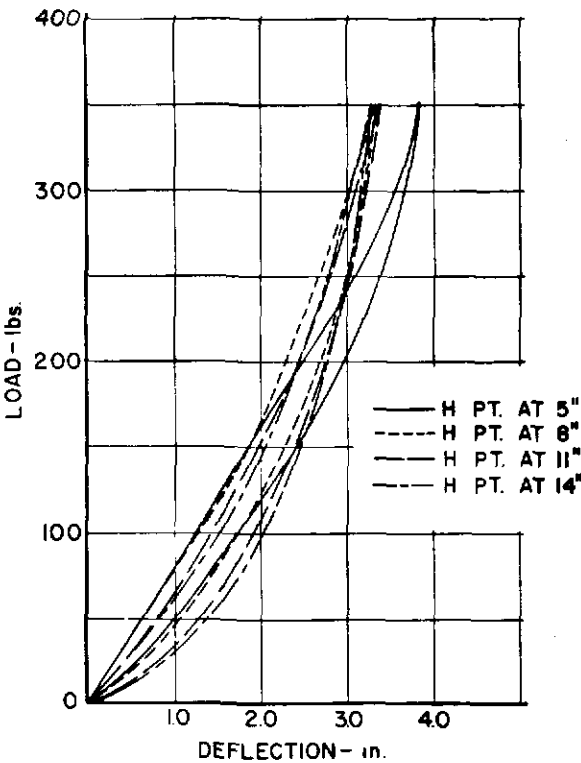


Fig. 13 - Load-deflection characteristics of the dummy-seat combination for different positions of the dummy on the seat

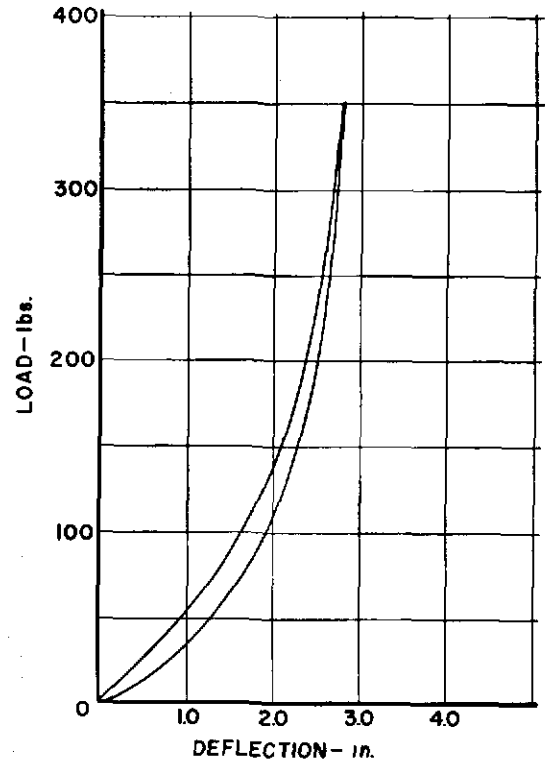


Fig. 14 - Load-deflection characteristics of the dummy-seat back combination

Table 2 - Position of Dummy on Sled

Dimension	Run Number														
	6	7	8	10	11	12	13	14	15	16	17	18	20	21	22
A	11.7	11.5	11.6	11.2	11.8	11.5	10.9	11.3	11.3	11.3	11.3	10.9	11.2	10.9	11.3
B	42.1	42.1	42.4	43.3	43.0	42.4	43.4	42.4	42.5	43.3	43.3	41.5	42.5	41.5	44.5
C	*	28.0	28.3	28.9	28.0	28.0	29.4	28.3	28.5	28.5	28.5	26.9	28.0	27.0	29.7
D	18.8	19.0	17.9	18.4	18.9	18.9	18.3	18.8	18.8	18.6	18.6	19.2	18.6	19.5	19.5
E	*	*	*	*	*	*	19.5	*	*	*	*	*	*	*	*
F	*	*	*	*	*	*	4.5	4.5	4.5	4.5	4.5	*	*	*	*
G	14.8	15.0	14.8	14.5	14.5	14.4	4.5	4.5	4.5	4.5	4.5	14.5	**	**	**
H	**	**	**	**	**	**	16.0	16.5	16.5	16.5	16.5	*	**	**	**
I	**	**	**	**	**	**	11.5	12.5	12.0	13.0	13.0	12.3	**	**	**
J	**	**	**	**	**	**	7.5	7.5	7.6	6.5	7.0	7.5	**	**	**
K	*	15.6	15.9	16.9	16.8	16.4	**	**	**	**	**	**	18.8	**	**
L	*	11.3	10.4	11.8	11.4	11.4	**	**	**	**	**	**	15.0	**	**
M	*	*	*	*	*	*	*	*	*	*	*	*	*	*	*
N	10.5	28.0	28.0	27.0	26.0	27.5	23.0	25.0	28.0	27.0	23.0	29.0	30.0	34.0	29.0
O	27.0	*	57.5	54.0	57.0	57.0	48.0	54.0	54.0	52.0	54.0	55.0	58.0	63.0	57.0
P	57.0	*	*	*	*	*	*	*	106	108	104	107	106	112	96.5
Q	*	110	108	110	113	112	104	*	106	*	*	*	*	*	*
R	106	**	**	**	**	**	25.0	23.0	28.0	23.0	22.0	26.0	**	**	**
S	**	38.0	38.5	40.0	37.5	37.0	39.0	38.0	37.0	39.0	37.0	34.0	**	**	**
T	*	**	**	**	**	**	55.0	56.0	55.0	56.0	54.0	55.0	**	**	**
U	**	**	**	*	13.8	13.5	55.0	56.0	55.0	56.0	54.0	55.0	**	**	**
VS	13.8	13.8	13.8	*	13.8	13.5	*	*	*	13.8	13.8	13.8	13.0	13.0	13.0
WS	20.5	20.5	20.8	21.5	21.5	23.5	23.5	23.5	23.0	21.8	25.8	22.0	14.4	14.8	14.5
XS	16.0	15.5	15.3	16.5	17.5	19.3	19.5	19.5	18.0	16.8	19.0	19.3	8.3	7.5	8.3

NOTES: Angles in degrees and linear dimensions in inches.

See Fig. 15 for location of dimensions.

*Not recorded.

**Not used.

remaining essentially constant for all of the runs. Figure 15 is a drawing of the dummy and sled with dimensions that were recorded for each run indicated. The measurements for each run are listed in Tables 2 and 3.

Prior to being put on the seat, the

dummy joints were adjusted to a predetermined torque*. Torque adjustments for each run are shown in Table 4.

*The torque varied with joint movement.

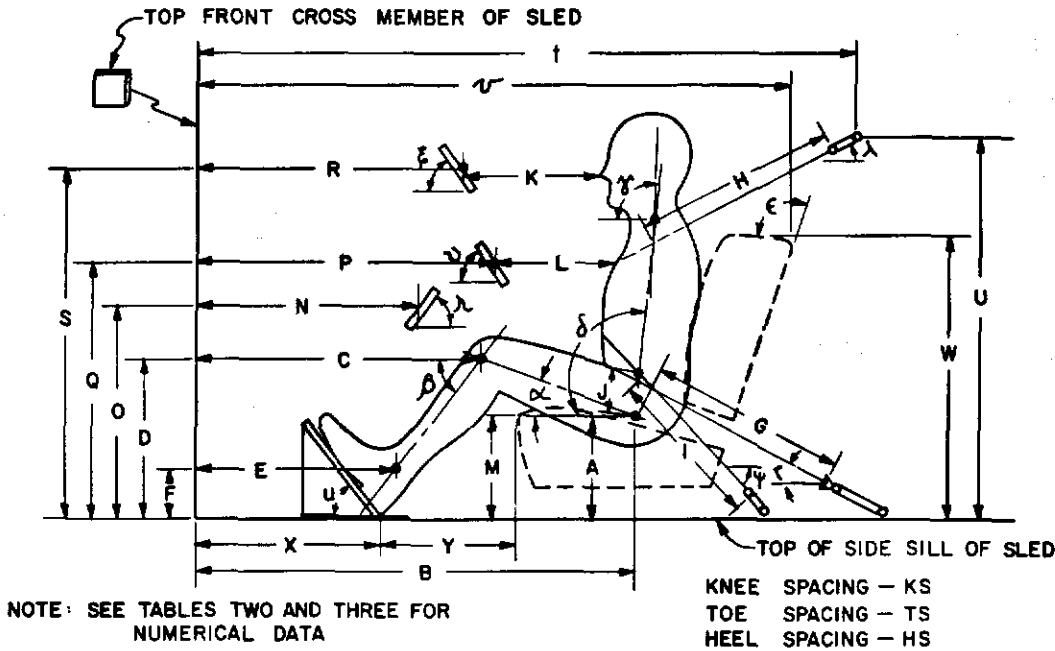


Fig. 15 - Drawing showing dummy and target setup dimensions

Table 3 - Location of Physical Components on the Sled

Lap Belt Configuration, Runs 6-12

P: 34"	R: 29"	V: 59"	Y: 12 3/4"
Q: 24 7/8"	S: 33 1/2"	W: 29 5/8"	μ: 50°
ν: 56°	ξ: 56°	X: 17 1/2"	ε: 104°

Lap and Diagonal Chest Belt Configuration, Runs 13-18

T: 66 1/2"	V: 59"	X: 17 1/2"	μ: 50°
U: 40 1/2"	W: 29 5/8"	Y: 12 3/4"	ε: 104°

Unrestrained Configuration, Runs 19-22

N: 23 1/2"	P: 30 1/2"	R: 24 7/8"	V: 59"	Y: 12 3/4"
O: 20 1/2"	Q: 26"	S: 35 1/4"	W: 29 5/8"	μ: 50°
η: 62°	ν: 65°	ξ: 56°	X: 17 1/2"	ε: 104°

NOTES:

1. Numbers are average values of the measured quantities. No changes in position were made during the evaluation of any given configuration.
2. See Fig. 15 for location of dimensions.
3. Dimensions given are the only ones pertinent to the particular configuration.

Table 4 - Dummy Joint Torques

Run No.	Knee		Hip		Shoulder		Spine		Neck	
	Before	After	Before	After	Before	After	Before	After	Before	After
5	28/28	*	26/26	*	8.7/8.7	*	14	*	7	*
9	*	24/28	*	15/21	*	7.3/7.3	*	14	*	7
10	24/28	26/26	26/27	25/29	7.3/7.3	7.3/8.0	16	18	7	8
11	26/26	*	26/29	*	7.3/8.0	*	18	*	8	*
12	26/26	32/38	26/29	24/33	7.3/8.0	6.0/6.0	18	16	8	7
13	27/27	*	26/26	*	9.5/10	*	16	*	7	*
15	*	34/27	*	27/26	*	10.5/10.5	*	17	*	5
16	28/28	*	27/27	*	10.5/10.5	*	16	*	7	*
18	*	36/29	*	27/27	*	7/9	*	10	*	7
19	28/28	*	27/27	*	9.5/9.5	*	16	*	7	*
22	*	24/28	*	34/35	*	9.5/9.5	*	7	*	7

NOTES:

1. Right side/Left side
2. * - Torques not checked
3. Elbow joints locked for all runs.
4. Joints not checked before or after Runs 6, 7, 8, 14, 17, 20, and 21.
5. All torques given in inch-pounds.

Table 5 - Summary of Experimental Program

Run No.	Velocity (mph)	Sled Acceleration (G's)	Total Stopping Distance (inches)	Restraint
6	10.3	9.2	4.6	Lap Only
7	9.9	10.0	4.5	Lap Only
8	9.9	9.8	4.5	Lap Only
10	20.2	19.8	9.7	Lap Only
11	20.1	19.6	10.0	Lap Only
12	20.1	20.0	10.0	Lap Only
13	10.0	11.0	5.0	Lap & Chest
14	10.0	9.9	4.9	Lap & Chest
15	9.9	10.3	5.0	Lap & Chest
16	20.1	23.0	10.4	Lap & Chest
17	20.1	24.4	9.8	Lap & Chest
18	19.8	24.0	10.2	Lap & Chest
20	10.0	10.0	5.1	Unrestrained
21	9.9	10.7	4.7	Unrestrained
22	19.5	22.2	10.7	Unrestrained

The load cells were located in the correct position to obtain the desired impact. For the unbelted condition four load cell targets were used--one for each knee, one for the chest, and one for the head. For the lap-belt-only condition the chest and head targets were positioned for impact. For the combined lap and cross chest restraint condition the targets were not used. All transducers were calibrated electronically prior to each day's runs.

The summary of the experimental program is shown in Table 5. Three runs were made at 10 miles per hour lap belted, 10 miles per hour lap and cross chest belted, 20 miles per hour lap belted, and 20 miles per hour lap and cross chest belted with all conditions as nearly identical for each series of three runs as possible.

Run Nos. 20 and 21 were both at 10 miles per hour. The standard dummy position was used in Run No. 20. For Run No. 21 the dummy was placed on the sled with no attempt made to duplicate the position used in previous runs. The purpose of this run was to determine whether the exact positioning used in the other runs was important.

Run Nos. 1 through 5 were used to establish techniques, and no records were obtained on Run Nos. 9 and 19. Consequently, these runs are not included in the data presented.

RESULTS

1. Typical records for each of the velocity and restraint conditions are shown in Figs. 16 through 22. These are photographic reproductions of the records and consequently provide the correct temporal and signal magnitude relationship for all transducers. There are two records for each run since the large number of signals precluded recording all traces on a single recorder. The sled acceleration trace is included on both of the records to serve as an index for establishing the time identity between the two records.

2. The important peak forces and accelerations are tabulated in Tables 6 through 11 and have been tabulated with the multiple reliability runs in adjacent columns for easy comparison. Since the peak readings of all of the transducers did not occur simultaneously, the peaks are recorded in the columns so headed together with the time at which these peaks occurred, and the readings of the other transducers are listed for the same time.

3. Biaxial head, chest, and femur accelerations, which are the absolute accelerations of the head and chest in the A-P and S-I directions and of the femur in the axial and perpendicular to the axial directions, can be observed on the records. It should be noted that these are absolute values, and the directions vary with the angular position of the head. The peak values of the A-P and S-I accelerations are shown in Tables 6 through 11.

4. The load-deflection characteristics of the lap belt (No. 4) and the cross chest belt (No. 2) are shown in Fig. 6. The data presented in Fig. 7 depicts the load-deflection characteristics of the webbing material over a wide range of loading conditions.

5. The static and dynamic load-deflection characteristics of the 4-inch thick honeycomb material for the head, chest, and knee impact are presented in Figs. 8 through 10.

6. The loads at each end and the total belt load for the lap-belt-only condition for the 10 and 20 mile per hour runs are shown in Figs. 23 and 24. The same data are presented in Figs. 25 and 26 for the lap plus cross chest restraint. The total belt loads for the four runs (10 and 20 mile per hour lap and lap plus cross chest) are shown in Fig. 27.

7. Tables 6 through 11 show the peak forces and accelerations for the three reliability runs at the 10 mile per hour lap belt restraint; 20 mile per hour lap belt restraint; 10 mile per hour lap plus cross chest restraint; and 20 mile per hour lap plus cross chest restraint. The data for the three runs are in adjacent columns for easy comparison.

8. Table 12 shows the average peak loads and accelerations for the three restraint conditions for the nominal 10 mile per hour 4-inch stopping distance and the nominal 20 mile per hour 9-inch stopping distance.

9. A graphical representation of the dummy position at discrete time intervals after impact is presented in Fig. 28 for each of the restraint conditions at 20 miles per hour impact velocity.

DISCUSSION AND ANALYSIS

While one of the main objectives of this program was to compare the forces and loads under similar conditions for 10 and 20 mile per hour unrestrained, lap belt, and lap and diagonal chest belt restraint systems, it was necessary to modify the position of the targets for the different conditions. The head and chest targets had to be changed between the lap belted and the unrestrained condition due to the difference in trajectory with the lap belt in place. The targets were moved out of the way for the full restraint condition in order to measure the total loads in the restraint system without any other external forces applied. Due to the change in target position, a comparison of the target forces for the three restraint conditions must be done with the understanding that the targets were not positioned the same for all runs. An attempt was made to maintain the direction of motion normal to the target prior to impact. This was not always achieved. Also, the impact was not always to the center of the targets as can be observed from Fig. 28.

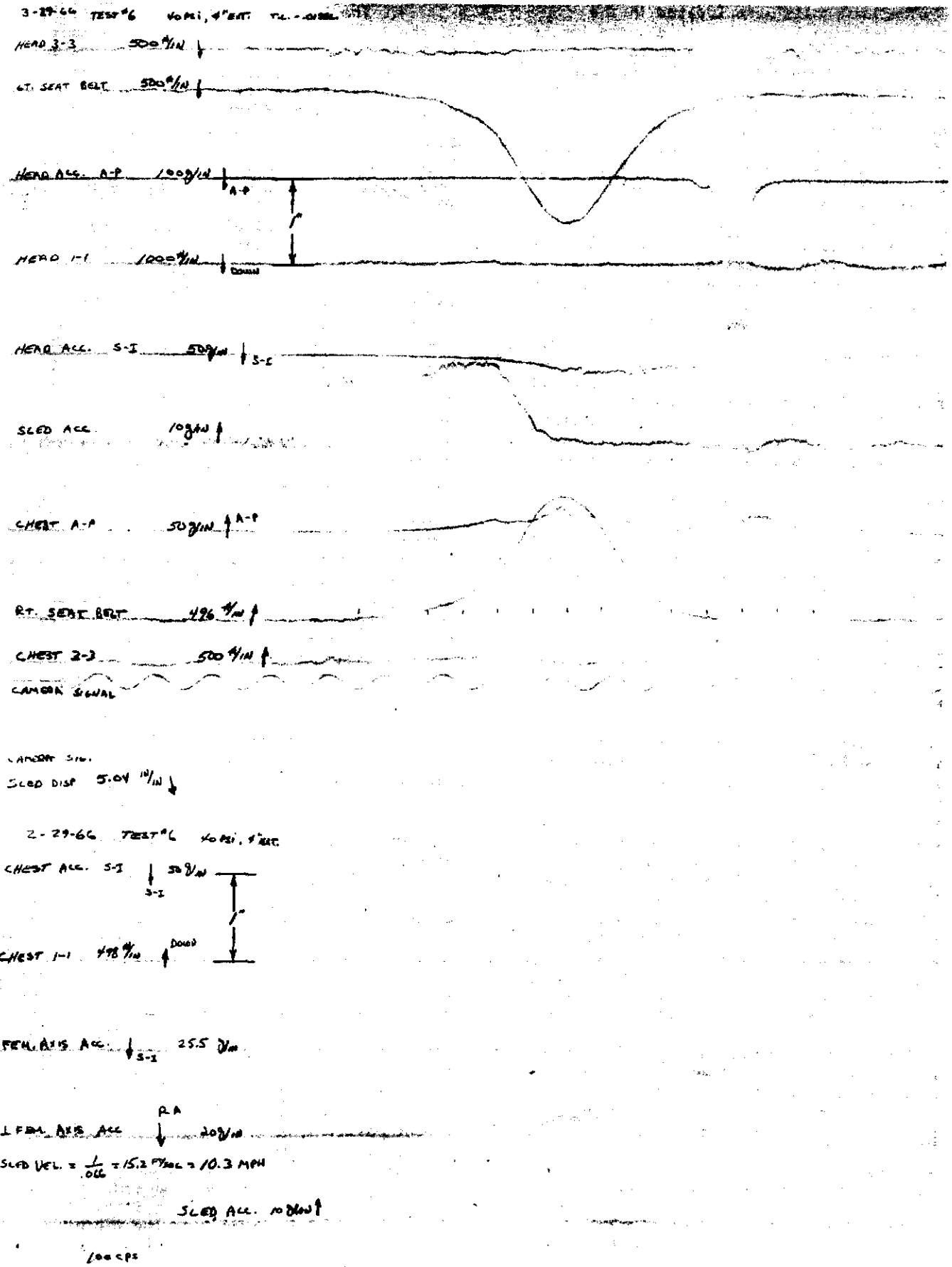


Fig. 16 - Reproductions of the experimental records for Run No. 6, lap belt only, at 10 mph

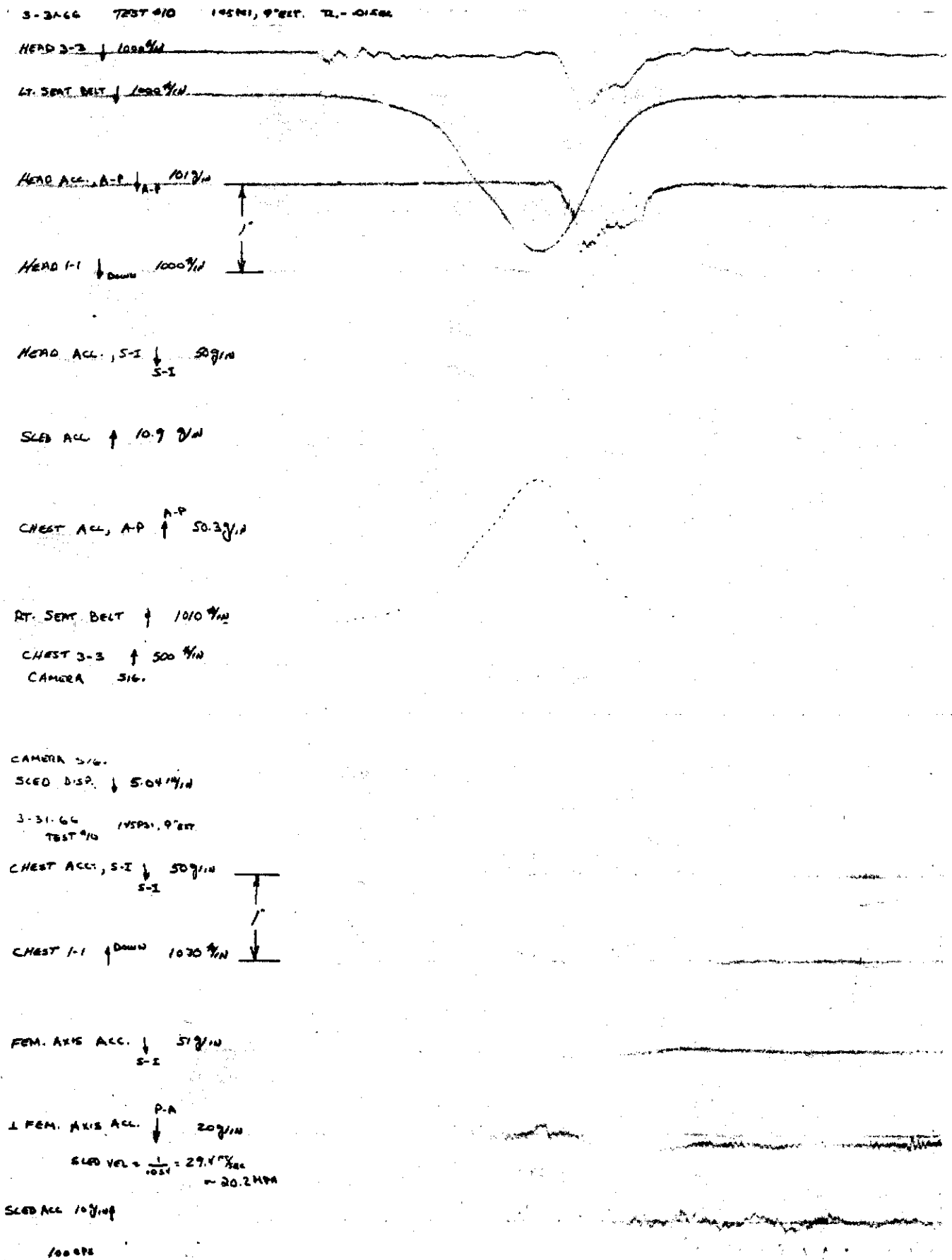


Fig. 17 - Reproductions of the experimental records for Run No. 10, lap belt only, at 20 mph

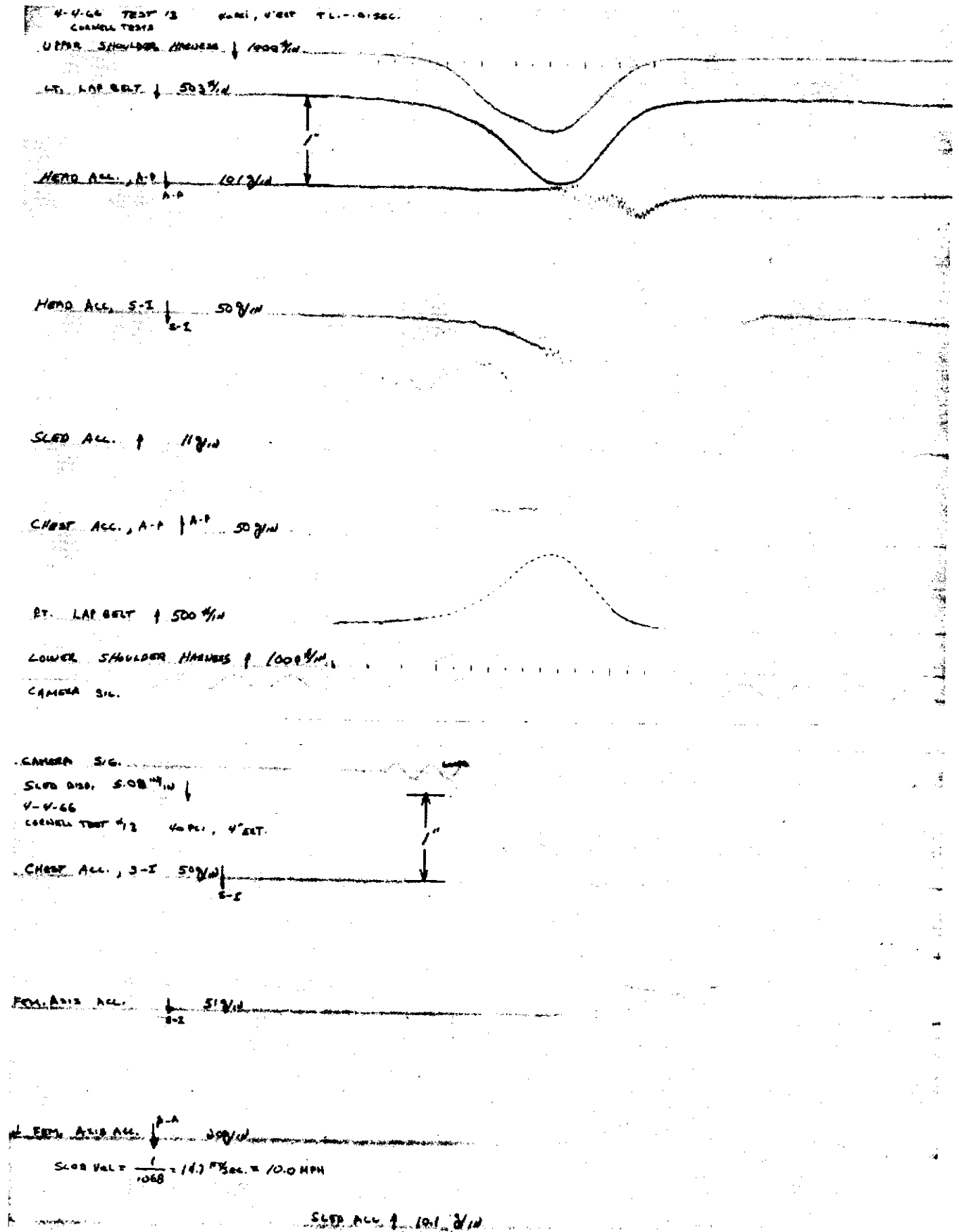


Fig. 18 - Reproductions of the experimental records for Run No. 13, lap and diagonal chest belt, at 10 mph

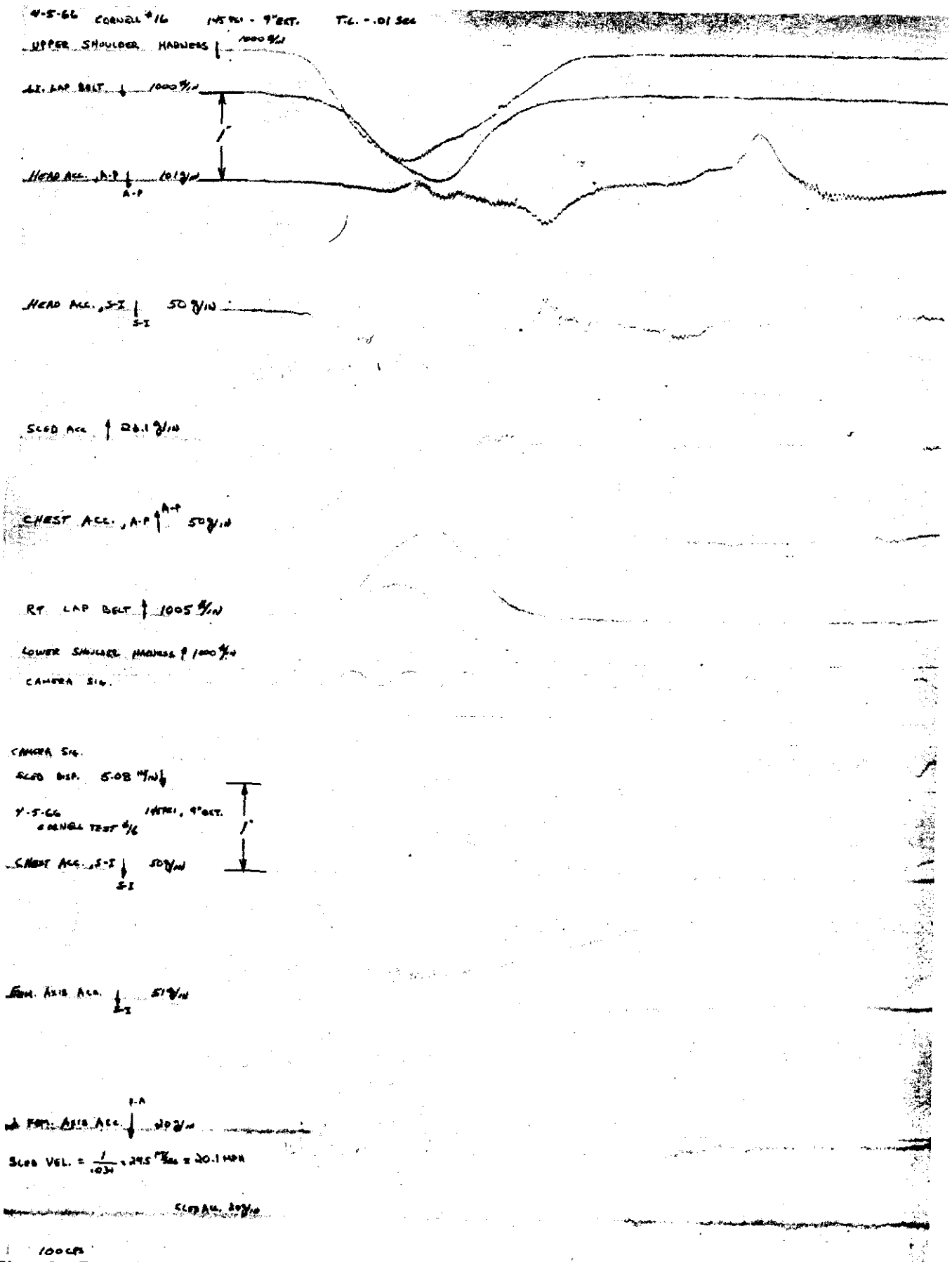


Fig. 19 - Reproductions of the experimental records for Run No. 16, lap and diagonal chest belt, at 20 mph

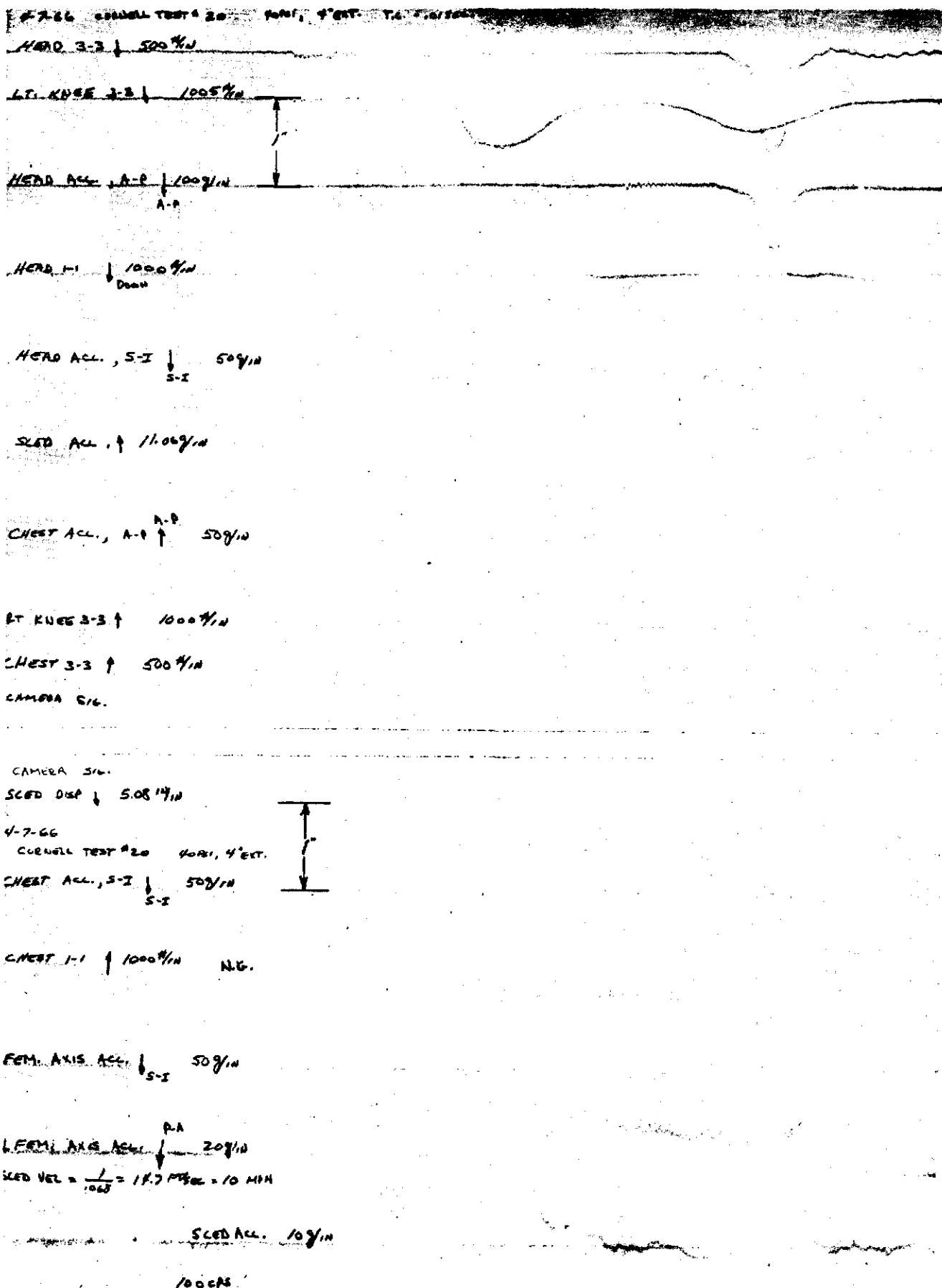


Fig. 20 - Reproductions of the experimental records for Run No. 20, unrestrained, at 10 mph

4-7-66 CORNELL TEST #21 40PSI, 4" EXT. T.L. - .0156"

HEAD 3-3 500 g/in

RT. KNEE 3-3 1005 g/in

HEAD ACC. A-P 100 g/in

HEAD 1-1 1000 g/in

HEAD ACC. S-I 50 g/in

SEED ACC. 11.06 g/in

CHEST ACC. A-P 50 g/in

RT. KNEE 3-3 1000 g/in

CHEST 3-3 500 g/in

CAMERA SIG.

CAMERA SIG
SEED DISP. 5.08 in

4-7-66 CORNELL TEST #21 40PSI, 4" EXT.
CHEST ACC. S-I 50 g/in

FEM. AXIS ACC. 50 g/in

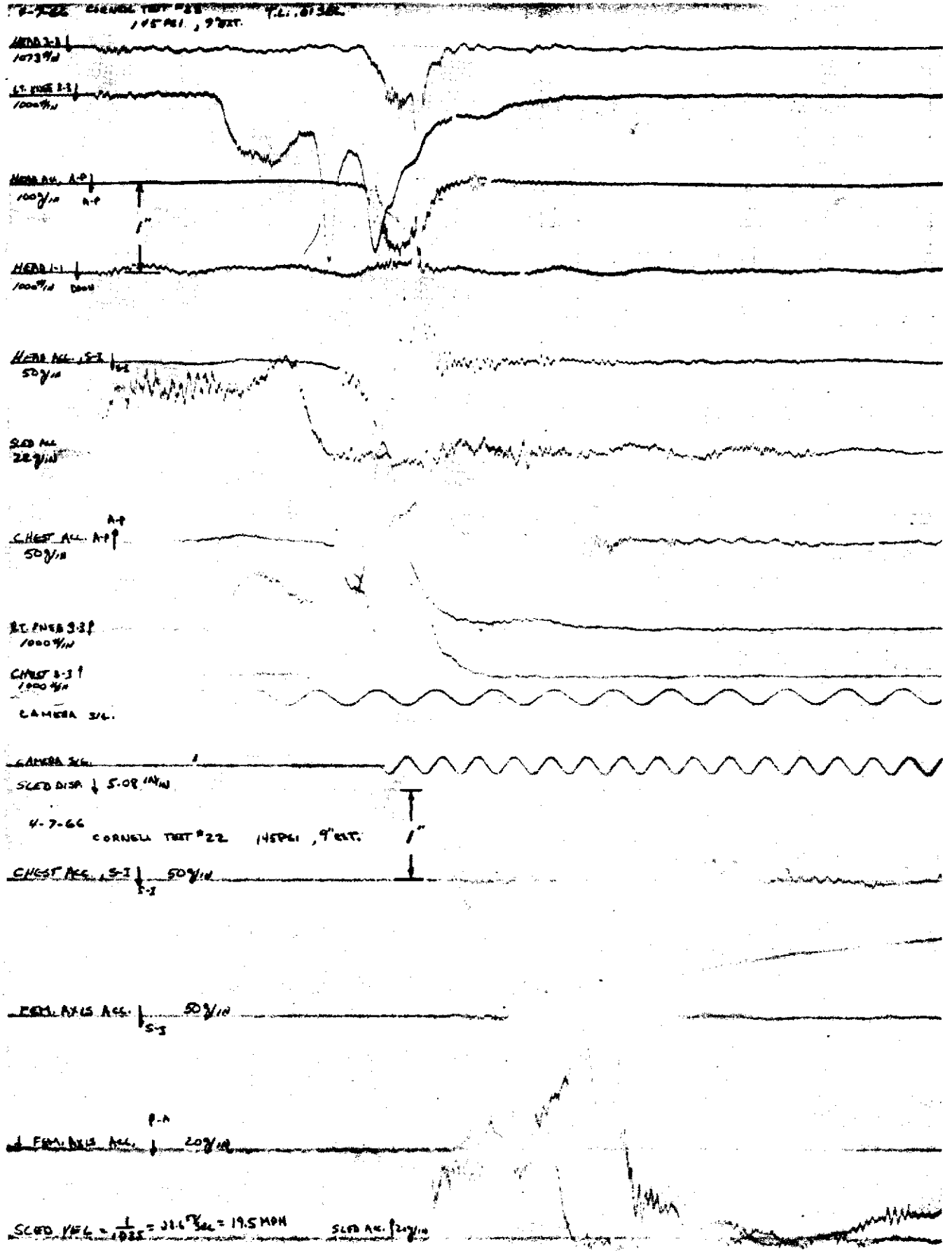
FEM. AXIS ACC. 20 g/in

SEED VEL. $\frac{1}{100} = 11.5 \text{ m/s} = 2.9 \text{ MPH}$

SEED ACC. 10 g/in

100 GPK

Fig. 21 - Reproductions of the experimental records for Run No. 21, unrestrained, at 10 mph, non-uniform position



100 LPS

Fig. 22 - Reproductions of the experimental records for Run No. 22, unrestrained, at 20 mph

TABLE 6 - Seat-Belted Dummy - 10 Mile Per Hour Run.
Loads and Accelerations Corresponding to Various Peak Loading Conditions

Run No.	Right Seat Belt Load	Left Seat Belt Load	Chest Acc. A-P Direction	Head Load 3-3 Direction	Chest Load 3-3 Direction
Time (ms)	68	65	68	118	123
Head 1-1 (#)	0	0	0	-30	-20
Head 3-3 (#)	0	20	0	485	400
Head A-P (g)	0	0	0	65.7	30.0
Head S-1 (g)	8.5	7.9	8.5	-20.0	-7.0
Chest 1-1 (#)	0	45	0	90	60
Chest 3-3 (#)	10	5	10	255	300
Chest A-P (g)	14.0	13.0	14.0	5.0	6.0
Chest S-1 (g)	9.0	4.1	9.0	1.0	0
Right Seat Belt (#)	695	670	695	5	0
Left Seat Belt (#)	750	725	750	35	25
Fem. Acc. S-1 (g)	-14.3	-14.6	-14.3	4.6	7.1
Fem. Acc. A-P (g)	3.6	3.8	3.6	0.6	1.2

NOTES: Negative sign indicates that the direction is opposite to that given in heading.

* Cable open.

TABLE 7 - Seat-Belted Dummy - 20 Mile Per Hour Run.
Loads and Accelerations Corresponding to Various Peak Loading Conditions

Run No.	Right Seat Belt Load	Left Seat Belt Load	Chest Acc. A-P Direction	Head Load 3-3 Direction	Chest Load 3-3 Direction
Time (ms)	10 11 12	10 11 12	10 11 12	10 11 12	10 11 12
Head 1-1 (#)	65 60 62	65 60 64	65 62 68	78 87 78	70 71 70
Head 3-3 (#)	0 10 10	0 10 20	0 20 0	30 0 20	0 0 0
Head A-P (g)	0 30 0	0 30 10	0 30 100	630 670 500	0 80 200
Head S-1 (g)	0 2.0 3.0	0 2.0 6.0	0 3.0 11.0	72.0 66.0 62.0	4.0 8.1 21.0
Chest 1-1 (#)	25 25 24.8	25 25 24.3	25 24.0 20.3	7.5 -35 -13.9	25.5 19.0 19.3
Chest 3-3 (#)	60 -50 30	60 -51 30	60 0 60	60 120 60	40 90 -10
Chest A-P (g)	275 200 180	275 200 200	275 320 960	660 320 700	920 640 1000
Chest S-1 (g)	31.6 30.0 30.5	31.6 30.0 31.5	31.6 32.0 38.5	18.6 16.0 21.0	28.1 23.5 37.5
Right Seat Belt (#)	11.5 8.4 11.0	11.5 8.4 10.5	11.5 8.9 7.5	5.0 11.9 - 1.5	11.0 0 5.5
Left Seat Belt (#)	1670 1740 1750	1670 1740 1730	1670 1700 1515	980 190 660	1510 1170 1315
Fem. Acc. S-1 (g)	1790 1720 1820	1790 1720 1830	1790 1710 1700	1100 280 900	1670 1260 1525
Fem. Acc. A-P (g)	-25.5 -27.0 -27.0	-25.5 -27.0 -26.5	-25.5 -25.0 -20.0	- 8.0 - 9.0 - 2.5	-19.4 -24.0 -16.5
	11.6 14.0 10.6	11.6 14.0 10.0	11.6 14 2.0	4.0 - 1.2 4.2	0 14.0 12.0

NOTE: Negative sign indicates that the direction is opposite to that given in heading.

TABLE 8 - Seat-Belted and Shoulder-Harnessed Dummy - 10 Mile Per Hour Run.
Loads and Accelerations Corresponding to Various Peak Loading Conditions

Run No.	Lower Shoulder Harness Peak		Upper Shoulder Harness Peak		Right Lap Belt Peak		Left Lap Belt Peak		Head Acc. A-P Peak			
Time (ms)	13	14	15	13	14	15	13	14	15	13	14	15
Lower Shoulder Harness (#)	57	56	55	62	56	55	63	61	64	87	83	78
Upper Shoulder Harness (#)	550	490	600	520	490	600	490	400	420	0	40	100
Right Lap Belt (#)	365	385	375	410	385	375	420	400	445	50	60	135
Left Lap Belt (#)	455	470	445	490	470	445	500	500	510	80	120	160
Head Acc. A-P (g)	0	0	0	0	0	0	0	1.0	7.0	29.3	21.2	23.0
Head Acc. S-I (g)	15.0	15.0	18.5	17.5	15.0	18.5	20.0	21.0	24.5	-17.5	-14.0	-12.0
Chest Acc. A-P (g)	17.5	18.5	16.5	19.5	18.5	16.5	20.0	17.5	15.0	2.0	-2.0	3.0
Chest Acc. S-I (g)	1.5	3.5	1.0	1.0	3.5	1.0	0	2.5	3.5	3.0	4.5	0.5
Fem. Acc. S-I (g)	-11.2	-11.2	-11.5	-14.3	-11.2	-11.5	-14.8	-13.3	-15.0	-5.1	-4.1	-16.5
Fem. Acc. A-P (g)	3.0	3.8	4.2	2.6	3.8	4.2	2.4	2.4	5.2	1.0	0.6	-0.8

NOTE: Negative sign indicates that the direction is opposite to that given in heading.

TABLE 9 - Seat-Belted and Shoulder-Harnessed Dummy - 20 Mile Per Hour Run.
Loads and Accelerations Corresponding to Various Peak Loading Conditions

Run No.	16	17	18	16	17	18	16	17	18	16	17	18	16	17	18
Time (ms)	45	54	54	48	54	56	61	59	56	61	59	56	61	59	56
Lower Shoulder Harness Peak	16	17	18	16	17	18	16	17	18	16	17	18	16	17	18
Upper Shoulder Harness Peak	1240	1390	1370	1250	1390	1380	1080	1340	1380	1080	1340	1380	1080	1340	1380
Right Lap Belt (#)	845	1115	1110	900	1115	1120	1000	1205	1120	1000	1205	1120	1000	1205	1120
Left Lap Belt (#)	810	1200	1130	880	1200	1180	1000	1260	1180	1000	1260	1180	1000	1260	1180
Head Acc. A-P (g)	5.1	14.1	17.0	2.0	14.1	18.0	15.2	22.2	18.0	15.2	22.2	18.0	15.2	22.2	18.0
Head Acc. S-I (g)	26.5	41.0	31.0	25.0	41.0	34.0	43.0	41.5	34.0	43.0	41.5	34.0	43.0	41.5	34.0
Chest Acc. A-P (g)	34.5	33.5	36.0	35.5	33.5	35.5	26.0	20.5	35.5	26.0	20.5	35.5	26.0	20.5	35.5
Chest Acc. S-I (g)	2.5	14.5	5.9	5.0	14.5	6.4	8.0	19.5	6.4	8.0	19.5	6.4	8.0	19.5	6.4
Fem. Acc. S-I (g)	-16.8	-24.5	-21.2	-18.4	-24.5	-21.7	-21.4	-24.5	-21.7	-21.4	-24.5	-21.7	-21.4	-24.5	-21.7
Fem. Acc. A-P (g)	10.0	16.2	14.0	10.4	16.2	14.2	14.4	17.0	14.2	14.4	17.0	14.2	14.4	17.0	14.2
Head Acc. A-P Peak	16	17	18	16	17	18	16	17	18	16	17	18	16	17	18
Head Acc. A-P Peak	92	83	90	40	0	20	250	470	310	40	30	0	70	90	50
Head Acc. A-P Peak	45.5	45.5	44.0	45.5	45.5	44.0	45.5	45.5	44.0	45.5	45.5	44.0	45.5	45.5	44.0
Head Acc. A-P Peak	-7.0	-7.5	-4.0	-7.0	-7.5	-4.0	-7.0	-7.5	-4.0	-7.0	-7.5	-4.0	-7.0	-7.5	-4.0
Head Acc. A-P Peak	-6.0	0	-3.0	-6.0	0	-3.0	-6.0	0	-3.0	-6.0	0	-3.0	-6.0	0	-3.0
Head Acc. A-P Peak	-9.5	-12.0	-4.9	-9.5	-12.0	-4.9	-9.5	-12.0	-4.9	-9.5	-12.0	-4.9	-9.5	-12.0	-4.9
Head Acc. A-P Peak	-5.1	-3.6	-1.0	-5.1	-3.6	-1.0	-5.1	-3.6	-1.0	-5.1	-3.6	-1.0	-5.1	-3.6	-1.0
Head Acc. A-P Peak	-9.2	-7.6	-8.0	-9.2	-7.6	-8.0	-9.2	-7.6	-8.0	-9.2	-7.6	-8.0	-9.2	-7.6	-8.0

NOTE: Negative sign indicates that the direction is opposite to that given in heading.

The honeycomb material was chosen for use on the targets because of its high energy absorbing, approximately constant force-deformation characteristics. Even though it is far better than most padding materials in this respect, it does not have a perfectly flat force-displacement characteristic, which is optimum. The load-deflection characteristics for static and dynamic impacts with the dummy body component are shown in Figs. 8, 9, and 10. In Figs. 9 and 10 it will be observed that the force builds up to a maximum and then drops off over the remaining portion of the usable deformation, after which it is essentially bottomed out and force increases rapidly.

Two important factors must be considered in choosing an energy-absorbing material. The deflecting force within the effective range of deflection of the material should not be greater than the maximum force that the body component can withstand without injury. The area under the load-deflection curve of the material, which represents the energy-absorbing capacity of the material, should be a maximum within the effective deflection

range. To achieve this optimum condition, deflection must occur at a constant force level. The padding loses its effectiveness as a safe energy absorber (bottoms) when the effective range of deflection is reached, causing a rapid increase in the deflecting force which exceeds the tolerable level.

This phenomenon is illustrated in the 10 and 20 mile per hour runs in the unrestrained and lap belt conditions. Table 13 gives the peak loads for these conditions along with the approximate maximum force required to crush the honeycomb. For the 10 mile per hour runs the forces were low enough that the material was never bottomed out. In fact, in most cases the forces were well below the maximum, and while there was some honeycomb deformation, it was due primarily to the small initial area of contact with the head, chest, or knees.

The effects of inadequate thickness of padding material are illustrated in the 20 mile per hour unrestrained condition. The records for the head, chest, and knees are shown in Fig. 22 for this run. The records show the increase in force to the maximum with the typical slight drop-off in force

TABLE 10 - Unrestrained Dummy - 10 Mile Per Hour Run.

Loads and Accelerations Corresponding to Various Peak Loading Conditions

Run No.	Rt. Knee Load 3-3 Direction		Lt. Knee Load 3-3 Direction		Chest Load 3-3 Direction		Head Load 3-3 Direction	
	20	21	20	21	20	21	20	21
Time (ms)	58	49	58	49	128	120	138	134
Rt. Knee 3-3 (#)	580	550	580	550	240	230	200	160
Lt. Knee 3-3 (#)	530	595	530	595	370	320	330	190
Fem. Acc. S-I (g)	-18.0	-16.0	-18.0	-16.0	- 7.0	- 4.5	- 5.5	- 3.5
Fem. Acc. A-P (g)	4.2	5.6	4.2	5.6	4.2	4.2	3.8	5.6
Head 1-1 (#)	0	0	0	0	0	0	0	0
Head 3-3 (#)	0	25	0	25	55	10	560	485
Head Acc. A-P (g)	0	0	0	0	7.0	0	69.0	63.0
Head Acc. S-I (g)	- 1.0	0	- 1.0	0	11.0	8.5	-18	-20.0
Chest 3-3 (#)	10	30	10	30	625	710	505	155
Chest Acc. A-P (g)	2.5	0	2.5	0	14.5	11.0	10.0	2.5
Chest Acc. S-I (g)	0	0	0	0	0	1.0	1.5	7.0

NOTES: Negative sign indicates that the direction is opposite to that given in heading.

The dummy was not accurately positioned in the seat for Run No. 21.

TABLE 11 - Unrestrained Dummy - 20 Mile Per Hour Run.
Loads and Accelerations Corresponding to Various Peak Loading Conditions

	Rt. Knee Load 3-3 Direction 1st Peak	Lt. Knee Load 3-3 Direction 1st Peak	Rt. Knee Load 3-3 Direction 2nd Peak	Lt. Knee Load 3-3 Direction 2nd Peak	Chest Load 3-3 Direction	Head Load 3-3 Direction
Time (ms)	65	65	80	80	89	89
Rt. Knee 3-3 (#)	1590	1590	2070	2070	610	610
Lt. Knee 3-3 (#)	1870	1870	1500	1500	720	720
Fem. Acc. S-1 (g)	-25.0	-25.0	-39.5	-39.5	2.5	2.5
Fem. Acc. A-P (g)	19.6	19.6	39.4	39.4	6.8	6.8
Head 1-1 (#)	20	20	-60	-60	-60	-60
Head 3-3 (#)	0	0	335	335	1580	1580
Head Acc. A-P (g)	0	0	40.0	40.0	80.0	80.0
Head Acc. S-1 (g)	2.5	2.5	28.0	28.0	-12.5	-12.5
Chest 3-3 (#)	130	130	1510	1510	1910	1910
Chest Acc. A-P (g)	0	*	*	*	*	*
Chest Acc. S-1 (g)	5.0	5.0	-8.0	-8.0	-11.5	-11.5

NOTES: Negative sign indicates that the direction is opposite to that given in heading.

* Trace could not be read.

Table 12 - Average Peak Loads and/or Accelerations for the Three Restraint Conditions

Restraint Configuration	Average Peak Loads and/or Accelerations											
	10 Miles Per Hour						20 Miles Per Hour					
	Head lbs	Head (A-P) G's	Chest lbs	Chest (A-P) G's	Rt. Lap lbs	Lt. Lap lbs	Lower Shoulder lbs	Upper Shoulder lbs	Rt. Knee lbs	Lt. Knee lbs		
Unrestrained	560	69	625	14.5	---	---	---	---	580	530		
Lap Belt	510	68	180	13	670	715	---	---	---	---		
Lap and Chest	---	24	---	18.8	420	505	550	835	---	---		

Restraint Configuration	Average Peak Loads and/or Accelerations											
	10 Miles Per Hour						20 Miles Per Hour					
	Head lbs	Head (A-P) G's	Chest lbs	Chest (A-P) G's	Rt. Lap lbs	Lt. Lap lbs	Lower Shoulder lbs	Upper Shoulder lbs	Rt. Knee lbs	Lt. Knee lbs		
Unrestrained	1580	80	1910	*	---	---	---	---	2070	1870		
Lap Belt	600	67	850	35	1720	1780	---	---	---	---		
Lap and Chest	---	45	---	34	1110	1150	905	1340	---	---		

NOTES: ---: Does not apply.

*Trace could not be read.

followed by very fast rise in force typical of the load-deformation characteristics of this material. The knees further show a double hump curve, probably caused by the well-known impact-partial separation-impact associated with spring mass systems. For 20 mile per hour impact a thicker target material would be required if bottoming is to be avoided.

One of the major problems in reducing injuries from impact to the vehicle interior is illustrated in the comparison of the 10 and 20 mile per hour runs. Even with a 4-inch energy-absorbing material with better than average characteristics at forces approaching safe maximum, the material bottoms out at 20 miles per hour and is inadequate. It is essential that adequate deformation be provided at the force tolerance level to prevent bottoming at the design impact speed. A comparison of the knee loads (right and left knee axis 3-3) of Run Nos. 20 and 22 illustrate this point. In Run No. 20, Fig. 20, the 10 mile per hour impact velocity is not

sufficient to cause the knee to bottom out. In this run both knee loads are within the energy-absorbing range of the honeycomb material. In Run No. 22, Fig. 22, both of the knee targets bottomed out. This is evidenced by an initial part of the record similar to the lower velocity run followed by two high peaks indicating that the material bottomed with attendant high forces. Similar results were observed between the lap belted 20 mile per hour run and the unrestrained 20 mile per hour run, Run Nos. 10 and 22 for the head and chest. However, the directions of impact to the head and chest were not the same for these two runs, so no conclusions can be drawn regarding the relative magnitude of the impact forces for these two conditions.

The effect of distributing the force over a greater part of the body by means of the combined lap and diagonal chest belt is illustrated in Fig. 27. For the 10 mile per hour, lap belt only run, the total force on the lap belt is approximately 1400 pounds, while

Table 13 - Comparison of Peak Target Loads for the 10 and 20 Mile Per Hour Lap Belt and Unrestrained Condition Illustrating Bottoming of the Honeycomb Target Material.

Body Component	Approx. Max. Honeycomb Crush Strength, lbs	Peak Load - lbs			
		Lap Belt Only		Unrestrained	
		10 mph	20 mph	10 mph	20 mph
Head	700	510	600	560	1580
Chest	1000	180	850	625	1910
Right knee	700			580	2070
Left knee	700			530	1870

Table 14 - Maximum Change of Position of Various Components of the Dummy Taken Relative to Sled

Co-ordinate	Unrestrained		Lap Belt		Lap and Diagonal Belt	
	10 mph	20 mph	10 mph	20 mph	10 mph	20 mph
C.G. of head X-dir.	20.0	19.6	16.0	17.6	7.2	8.8
Shoulder point X-dir.	16.4	18.8	11.6	14.4	3.6	7.6
Hip point X-dir.	5.6	11.2	4.4	8.0	4.0	8.4
C.G. of head Y-dir.	1.6	1.2	5.6	7.2	5.6	11.2
Shoulder point Y-dir.	1.2	1.2	5.8	12.8	6.0	12.0
Hip point Y-dir.	2.0	1.6	1.6	3.2	1.6	1.6
Head rotation	24.0	9.0	38.0	24.0	59.0	55.0

NOTES:

Positive X - forward with respect to sled
Positive Y - downward with respect to sled

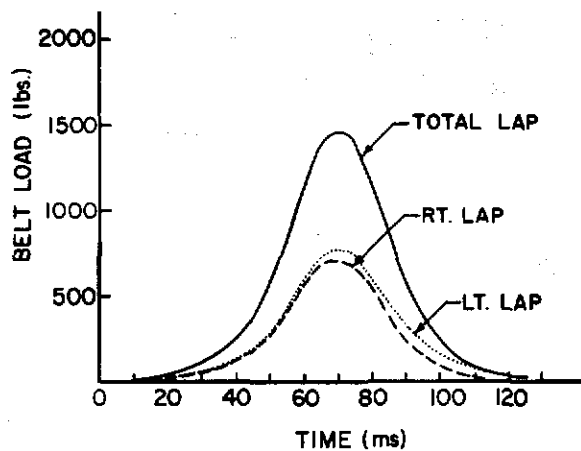


Fig. 23 - Belt loads for Run No. 6, lap belt, 10 mph

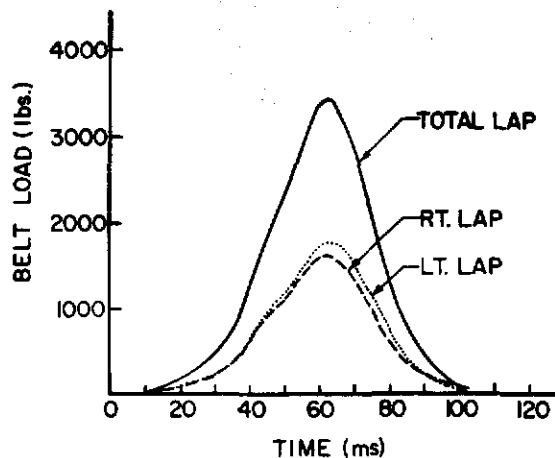


Fig. 24 - Belt loads for Run No. 10, lap belt, 20 mph

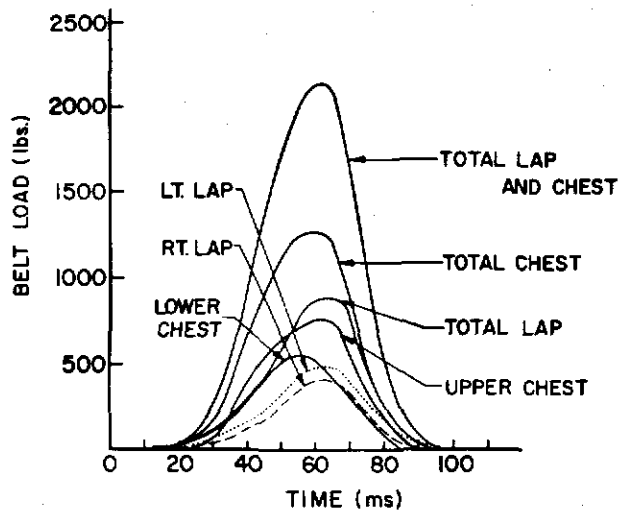


Fig. 25 - Belt loads for Run No. 13, lap and diagonal chest belt, 10 mph

for the 10 mile per hour, lap and diagonal chest, the total lap load is approximately 900 pounds. For the 20 mile per hour, lap belt only run, the total lap belt load was approximately 3500 pounds, while the lap belt load for the seat belt and diagonal chest belt condition was 2000 pounds. Thus, in addition to minimizing or eliminating

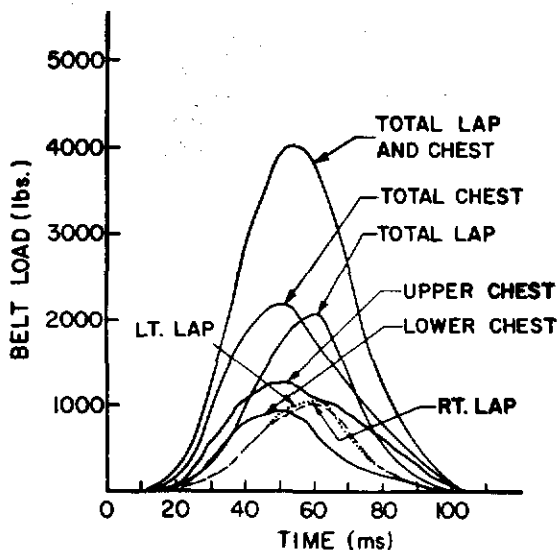


Fig. 26 - Belt loads for Run No. 16, lap and diagonal chest belt, 20 mph

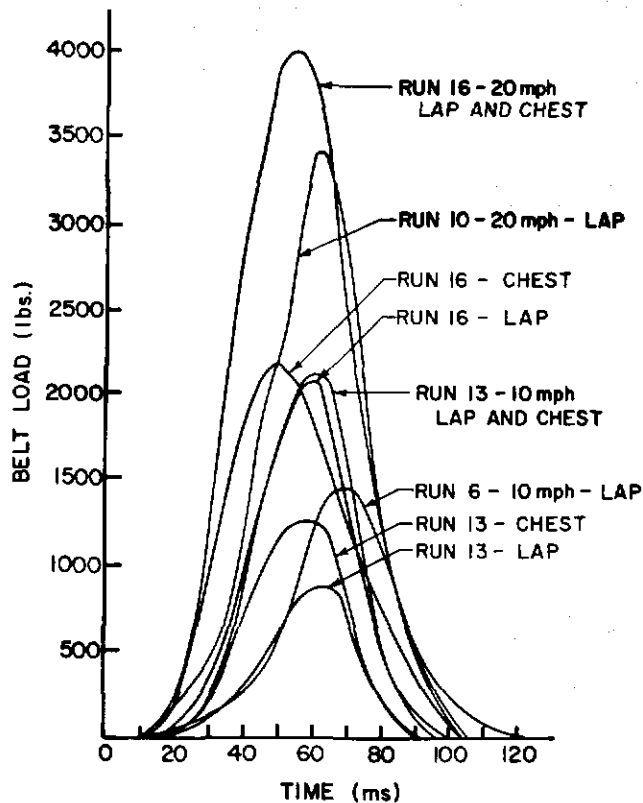


Fig. 27 - Summary of belt loads for the 10 and 20 mph lap and lap and diagonal chest belts

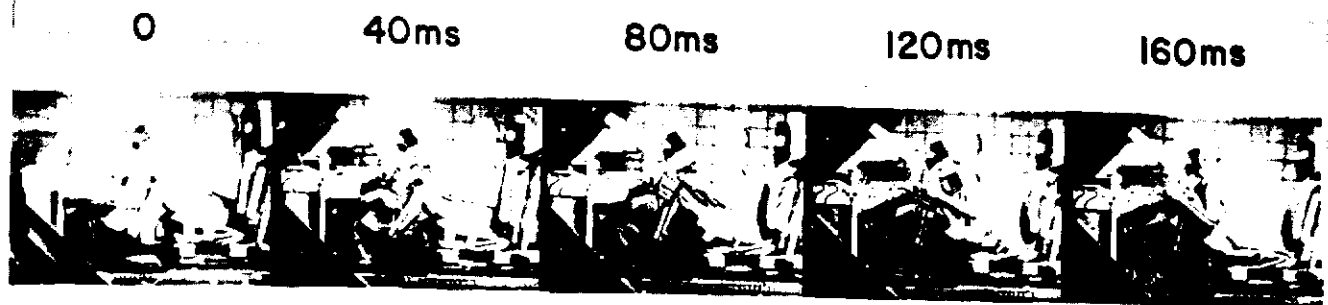
impact forces to the vehicle interior, the combined restraint system appreciably reduces the forces in the lap belt.

Photographs of the dummy at impact and 40, 80, 120, and 160 milliseconds after impact are shown in Fig. 28 for the unrestrained, lap belt, and lap and diagonal chest belt. For the unrestrained impact the dummy remained in an essentially upright position as it moved forward for the first 120 milliseconds, even though the knees were essentially bottomed out at this point and contact had been made with the chest target. The chest and head targets were both loaded unsymmetrically as shown in the 160 millisecond photograph. The targets were placed at too great an angle, since prior to

the runs it was assumed that there would be more angular body and head movement at the time of impact.

With the lap belt, the dummy remained in an essentially upright position as it moved forward for approximately 80 milliseconds, even though the peak seat belt loads occurred earlier. For this run the head impact was almost normal while the chest impact was at an angle. Also, the lap belt apparently pulled the hips back and the chest and head down so that the chin hit the top of the chest load cell. This occurred well after the peak forces were achieved.

With the lap and diagonal chest belt the dummy remained essentially upright as it moved forward for 80 milliseconds, after which it



UNRESTRAINED— RUN NO. 22



LAP BELT— RUN NO. 10



LAP AND DIAGONAL CHEST— RUN NO. 16

Fig. 28 - Comparison of dummy position and posture for equal time intervals after initial sled impact for the unrestrained, lap belt, and lap and diagonal chest belt runs at 20 mph

started to submarine and its shoulders were forced down by the diagonal chest belt. This agrees with Fredericks' findings (2) and disagrees with Bohlin's findings (3). The difference in the results between this investigation and those of Fredericks and Bohlin could be due to the difference in the dummy, the difference in the webbing materials, or the difference in the anchor positions. A thorough evaluation of all of the parameters affecting the restraint system is needed to establish the optimum configuration for the system.

A motion analysis was made from the high speed motion pictures including the X and Y components of the hip, shoulder, and head and the angle of the femur, tibia, and head. These data are presented in Figs. 29 through 37 for the 20 mile per hour runs. Figure 38 shows the cart displacement during the same time interval. Thus, in order to obtain the relative movement of the hip with respect to the cart during the decelerating stroke, it is necessary to subtract the cart displacement for any particular time from the X component for the same time. For example, for Run No.

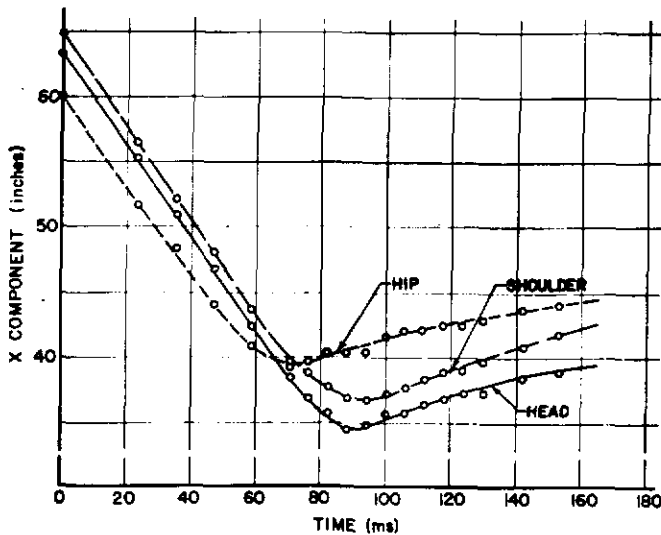


Fig. 29 - X component of the head, shoulder, and hip from high speed movies as a function of time for Run No. 22, unrestrained, 20 mph

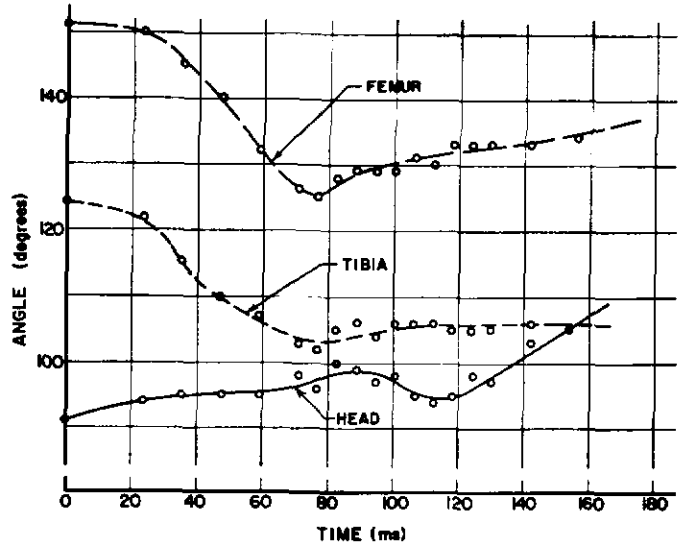


Fig. 31 - Angular position of the head, tibia, and femur as a function of time for Run No. 22, unrestrained, 20 mph

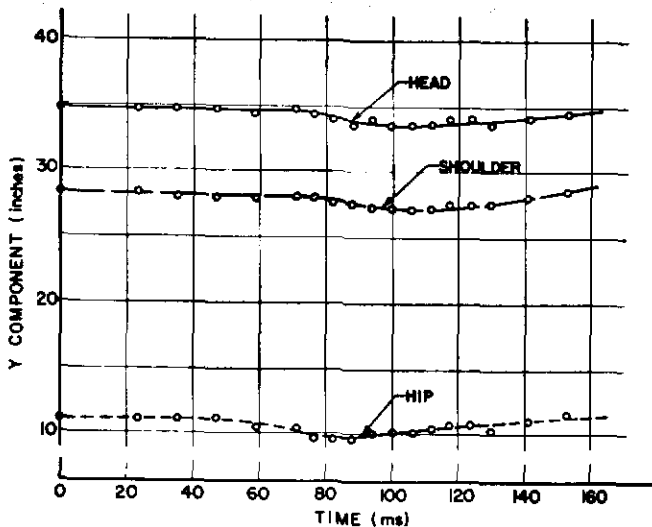


Fig. 30 - Y component of the head, shoulder, and hip from high speed movies as a function of time for Run No. 22, unrestrained, 20 mph

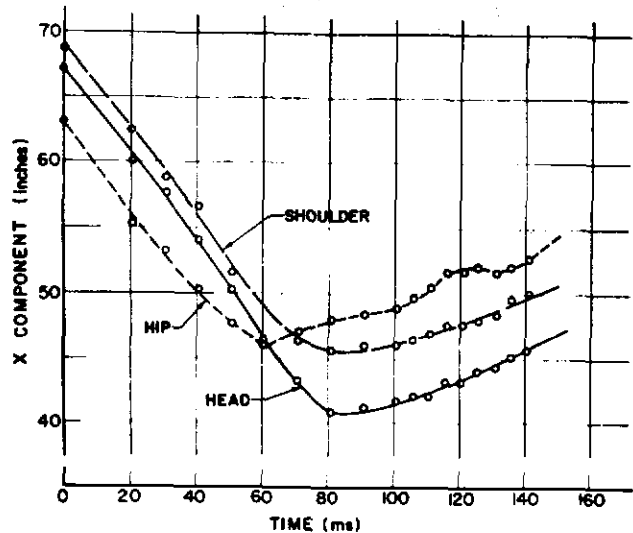


Fig. 32 - X component of the head, shoulder, and hip from high speed movies as a function of time for Run No. 10, lap belt only, 20 mph

10, lap belt only, 20 miles per hour, the maximum hip point displacement in the X direction was about 8 inches, which occurred at approximately 60 milliseconds (absolute X component 17 inches minus the 9-inch cart displacement). Similar calculations for the other runs are presented in Table 14. The angular motions are measured from the lines drawn on the head, tibia, and femur.

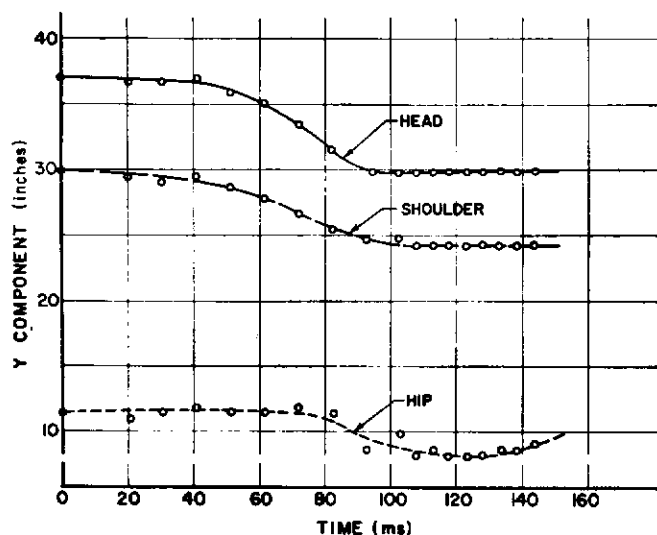


Fig. 33 - Y component of the head, shoulder, and hip from high speed movies as a function of time for Run No. 10, lap belt only, 20 mph

An attempt was made to obtain the impact acceleration by double differentiation of the time-displacement curves of the motion analysis. This was unsuccessful due to inadequate definition of the curve at impact caused by an insufficient frame rate. Camera speeds much higher than the 1000 frames per second will be required for a motion analysis of impact acceleration.

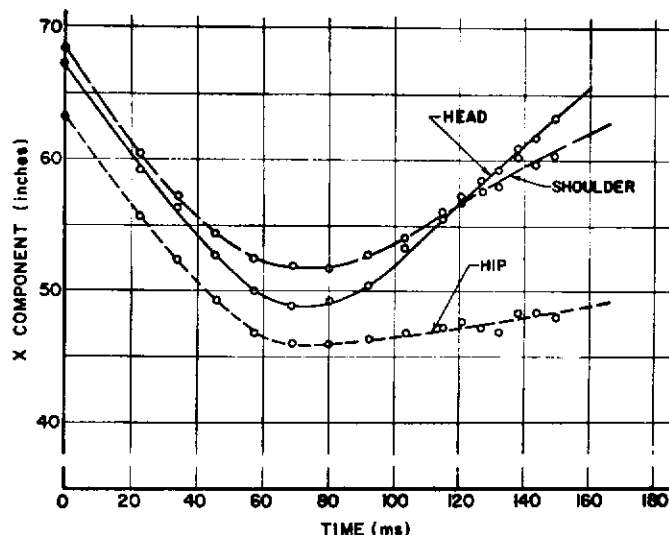


Fig. 35 - X component of the head, shoulder, and hip from high speed movies as a function of time for Run No. 16, lap and diagonal chest belt, 20 mph

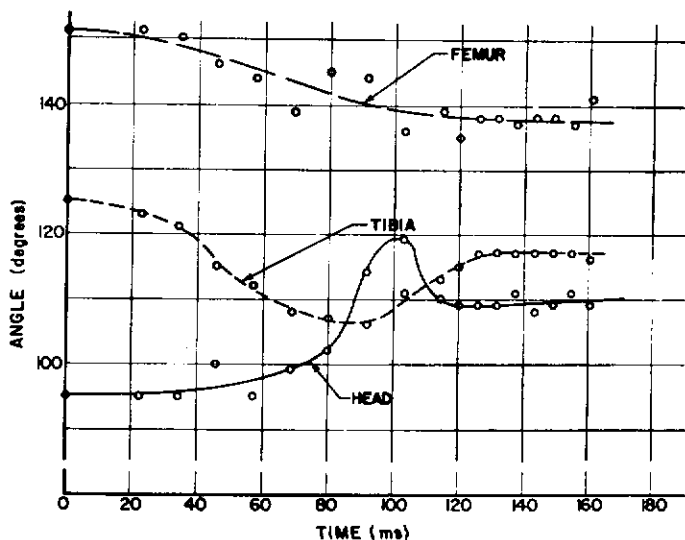


Fig. 34 - Angular position of the head, femur, and tibia as a function of time for Run No. 10, lap belt only, 20 mph

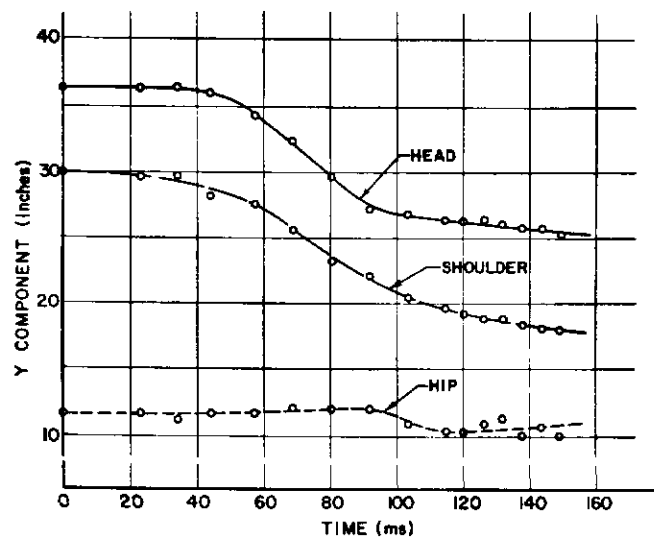


Fig. 36 - Y component of the head, shoulder, and hip from high speed movies as a function of time for Run No. 16, lap and diagonal chest belt, 20 mph

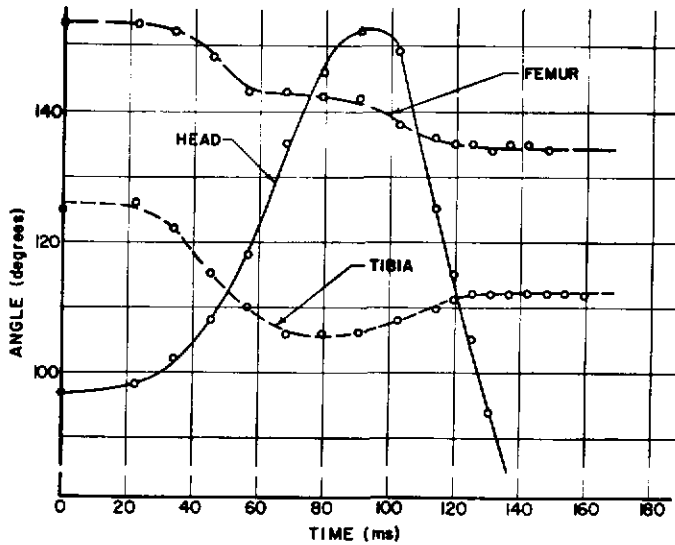


Fig. 37 - Angular position of the head, femur, and tibia as a function of time for Run No. 16, lap and diagonal chest belt, 20 mph

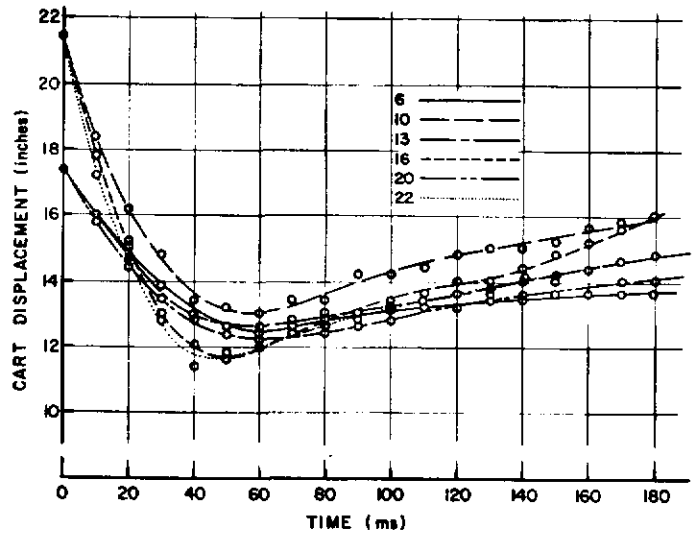


Fig. 38 - Cart displacement as a function of time

REFERENCES

1. Charles K. Kroell and Lawrence M. Patrick, "A New Crash Simulator and Biomechanics Research Program." Proceedings, Eighth Stapp Car Crash and Field Demonstration Conference, Detroit, Michigan: Wayne State University Press, 1966.

2. R. H. Fredericks, "Barrier Collision Investigation of Harness Restraining Systems." Proceedings, Seventh Stapp Car Crash Conference, Springfield, Illinois: Charles C. Thomas, 1965.

3. N. I. Bohlin, "Studies of Three-Point Restraint Harness Systems in Full-Scale Barrier Crashes and Sled Runs." Proceedings, Eighth Stapp Car Crash and Field Demonstration Conference, Detroit, Michigan: Wayne State University Press, 1966.